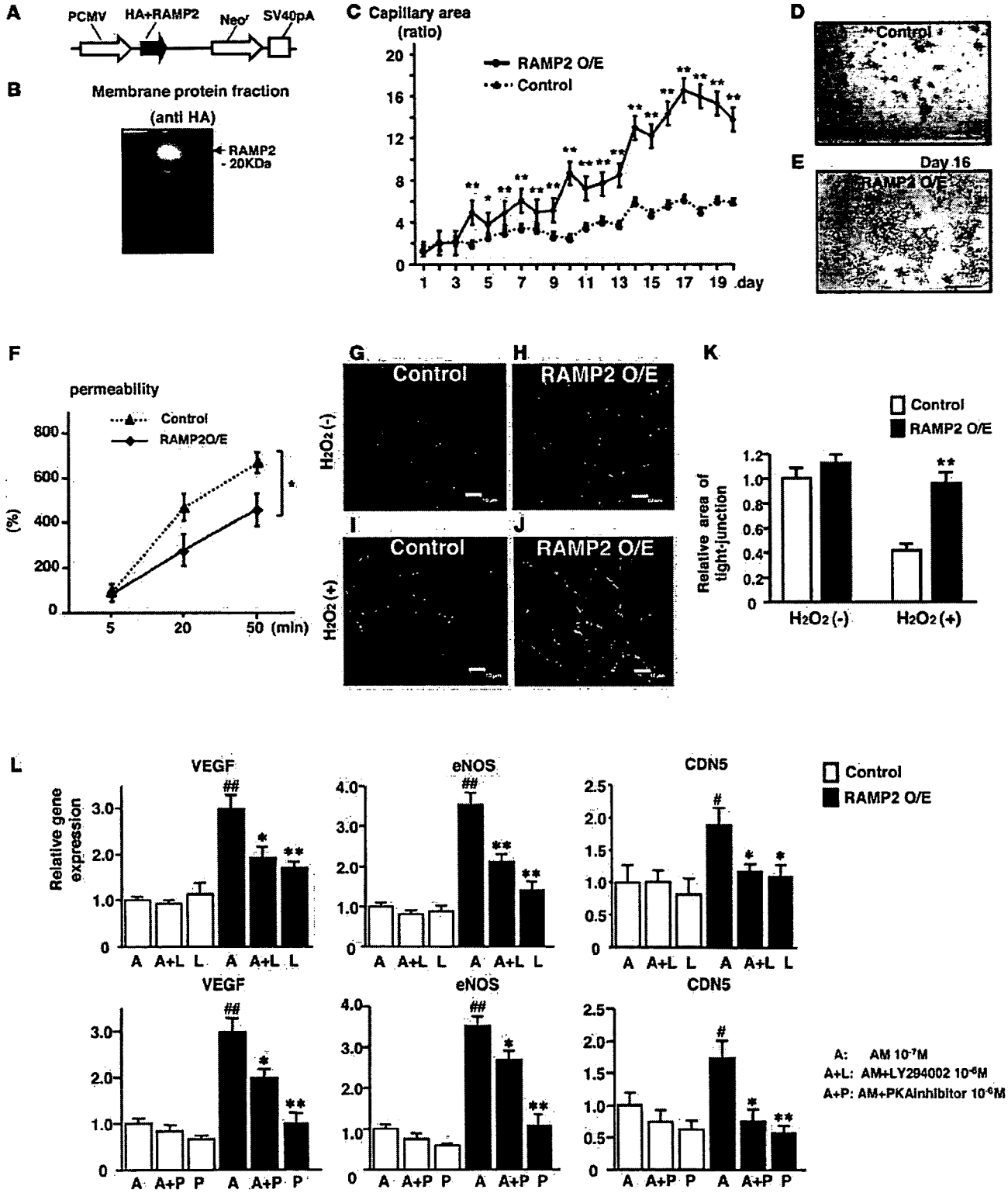
A
PCMV
HA+RAMP2
Neo'
SV40pA
B
Membrane protein fraction
(anti HA)
RAMP2
- 20KDa
C Capillary area
(ratio)
RAMP2 O/E
Control
day
D
Control
E
Day 16
RAMP2 O/E
F
permeability
Control
RAMP2O/E
(%)
5
20
50 (min)
G
Control
H
RAMP2 O/E
I
Control
J
RAMP2 O/E
H2O2 (-)
H2O2 (+)
K
Control
RAMP2 O/E
Relative area of tight-junction
H2O2 (-)
H2O2 (+)
L
VEGF
eNOS
CDN5
Relative gene expression
Control
RAMP2 O/E
A
A+L
L
A+P
P
A: AM 10-7M
A+L: AM+LY294002 10-6M
A+P: AM+PKAinhibitor 10-6M

Figure 4
Establishment and functional analysis of the RAMP2O/E line. (**A**) Plasmid vector used to overexpress RAMP2 (see Methods). (**B**) Western blot analysis of the membrane protein fraction from RAMP2O/E cells showing expression of the transfected gene. (**C–E**) Capillary formation by EAhy926 cells on Matrigel. RAMP2O/E cells or control ECs were cultured in 24-well culture plates coated with Matrigel in medium containing 10^{-7} M AM, and capillary formation was monitored microscopically. (**C**) Capillary area relative to day-1 cell surface area. RAMP2O/E cells exhibited greater angiogenesis than control. $n = 8$ per group. (**D** and **E**) Representative photomicrographs of RAMP2O/E and control cells. (**F**) In vitro vascular permeability assay (see Methods). The permeability of the monolayer, assessed using a fluorescence microplate reader, is expressed relative to control at 5 min. RAMP2O/E cells showed significantly lower permeability than control ECs. $n = 10$ per group. $^{*}P < 0.05$, $^{**}P < 0.01$ vs. control. (**G–J**) Immunostaining of ZO-1. ECs were cultured until confluent on chamber slides in the presence of 10^{-7} M AM. Two hours after treatment with 0.5 mM H_2O_2, the cells were immunostained using anti–ZO-1 antibody and Hoechst 33342. (**K**) Comparison of the tight junctions illustrated by the immunostaining in **G–J**. Tight junctions were better preserved after H_2O_2 treatment in RAMP2O/E cells than control ECs. $^{**}P < 0.01$ vs. H_2O_2-treated control; comparison in 4 microscopic fields each from 3 independent experiments. (**L**) Quantitative real-time PCR analysis of gene expression in ECs cultured on Matrigel. Values are relative to control ECs treated with 10^{-7} M AM. RAMP2O/E cells showed stronger expression of VEGF, eNOS, and CDN5 than control cells; this effect was blocked by LY294002 (10^{-6} M) or a PKA inhibitor (10^{-6} M). $n = 6$ per group. $^{\#\#}P < 0.01$ and $^{\#}P < 0.05$ vs. AM-treated control. $^{**}P < 0.01$ and $^{*}P < 0.05$ vs. AM-treated RAMP2O/E. Scale bars: 50 μm (**D** and **E**); 10 μm (**G–J**).

angiogenic effect was greatly diminished in explants from *RAMP2*$^{+/-}$ mice (Figure 5, B–E). Similarly, in Matrigel plug assays, *RAMP2*$^{+/-}$ mice showed reduced neovascularization in response to stimulation with bFGF (Figure 5, F and G). We also cultured tissue from the aorta-gonad-mesonephros (AGM) regions of E10.5 embryos, which were plated on mouse OP9 stromal cells to promote angiogenesis. We found that there was substantially less development of a vascular network in tissue from *RAMP2*$^{-/-}$ than WT mice (Figure 5, H and I).

Enhanced vascular permeability in adult RAMP2$^{+/-}$ *mice.* Based on the findings presented thus far, we hypothesized that the AM-RAMP2 system regulates vascular stability in adults as well as during development, which we tested by analyzing vascular permeability in adult *RAMP2*$^{+/-}$ mice. We initially generated a footpad edema model by subcutaneously injecting λ-carrageenan, a sulfated high-MW polygalactan. As expected, *RAMP2*$^{+/-}$ mice showed greater swelling than did WT mice (Figure 6A). We then directly measured vascular permeability using a skin edema model. Mice were injected with FITC-BSA via the tail vein as a tracer of vascular permeability, after which serum exudation caused by subcutaneous injection of histamine was measured using a fluorescence microplate reader. As shown in Figure 6B, *RAMP2*$^{+/-}$ mice exhibited greater vascular permeability than did WT mice.

Finally, to prove that the capacity of the AM-RAMP2 system to regulate vascular permeability could in fact make it a useful therapeutic target, we generated a brain edema model in which edema was caused by injuring the brain using a liquid nitrogen–cooled copper probe. Twenty-four hours after the injury, *RAMP2*$^{+/-}$ mice showed greater vascular permeability than did WT mice (Figure 6C), which suggests that the AM-RAMP2 system is important for maintenance of the blood-brain barrier.

Discussion

The mechanism by which a stable and functional vascular network is generated and regulated by humoral factors is still not fully understood. For example, VEGF alone is insufficient for stable vessel formation (36) and presents major disadvantages for thera-

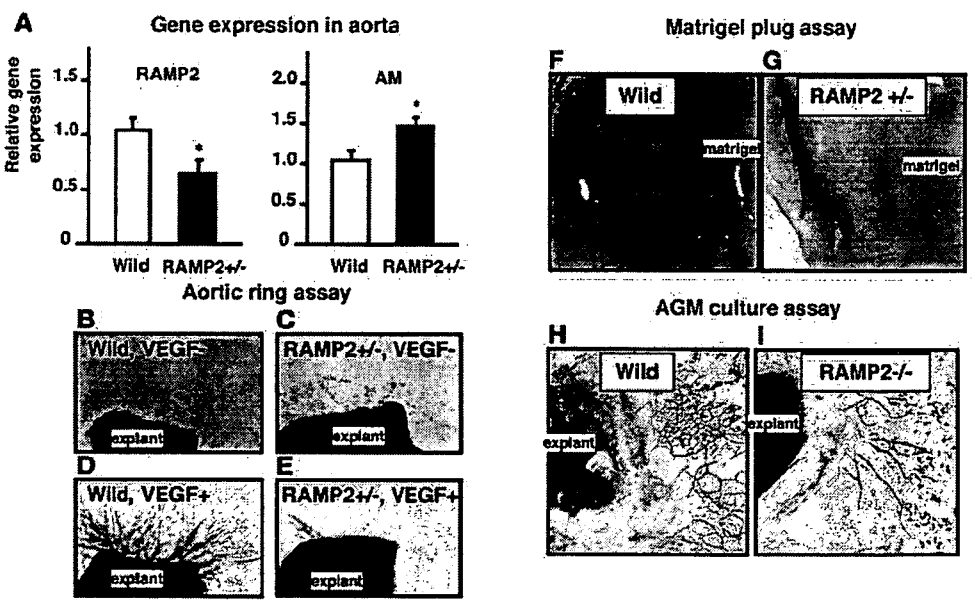

Figure 5
Reduced responses to angiogenic stimuli in adult *RAMP2*$^{+/-}$ mice. (**A**) Gene expression in aortas from 8-week-old WT and *RAMP2*$^{+/-}$ mice. Quantitative real-time PCR analysis of total RNA extracted. In *RAMP2*$^{+/-}$ mice, RAMP2 expression was about half that in WT mice, while AM expression was significantly upregulated. $n = 6$ per group. (**B–E**) Aortic ring assay. Representative photomicrographs of 7-day collagen gel cultures of aortas from 8-week-old mice (see Methods). Aortic explants from WT and *RAMP2*$^{+/-}$ mice were cultured in the absence or presence of VEGF (50 ng/ml), and capillaries sprouting from the edges of the rings were analyzed. The aortic explants from *RAMP2*$^{+/-}$ mice showed diminished angiogenesis. $n = 6$ per group. (**F** and **G**) Matrigel angiogenesis assay (see Methods). Representative photomicrographs showing angiogenesis in response to injected Matrigel. Capillary formation toward the Matrigel was greatly reduced in *RAMP2*$^{+/-}$ (**G**) compared with WT (**F**). $n = 6$ per group. (**H** and **I**) In vitro culture of AGM explant (see Methods). Representative photomicrographs showing the vascular network formation from the tissue cultured AGM region of E10.5 WT (**H**) and *RAMP2*$^{-/-}$ embryos (**I**). Vascular network formation was diminished in *RAMP2*$^{-/-}$ mice. $n = 4$ per group.

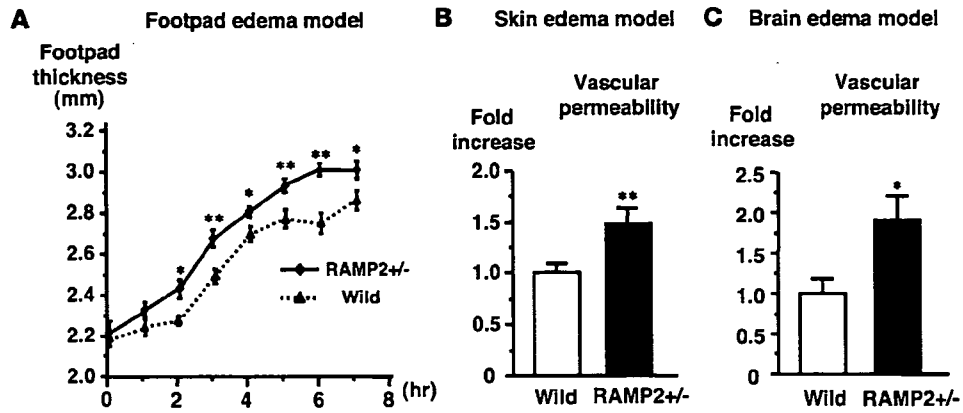

Figure 6

In vivo vascular permeability assay. (**A**) Footpad edema model. λ-Carrageenan was injected into the footpad of 8-week-old *RAMP2*$^{+/-}$ and WT mice to induce edema for the evaluation of vascular permeability in adult mice; swelling of the footpad was measured hourly using a thickness gauge. *RAMP2*$^{+/-}$ mice showed significantly greater swelling than WT mice. $n = 12$ per group. $^{**}P < 0.01$, $^{*}P < 0.05$ vs. WT. (**B**) Skin edema model (see Methods). Fluorescence intensity was measured using a fluorescence microplate reader. Permeability levels are presented relative to WT. *RAMP2*$^{+/-}$ mice ($n = 8$) showed significantly greater vascular permeability than WT mice ($n = 13$). $^{**}P < 0.01$ vs. WT. (**C**) Brain edema model (see Methods). Vascular permeability in *RAMP2*$^{+/-}$ mice ($n = 12$) is presented relative to that in WT mice ($n = 10$). *RAMP2*$^{+/-}$ mice showed significantly greater vascular permeability than WT mice. $^{*}P < 0.05$ vs. WT.

peutic angiogenesis, in that it increases vascular permeability and may exacerbate arteriosclerosis.

Studies of gene-targeted mice have led to the identification of angiogenic factors that had not previously been recognized for their angiogenic properties. AM was originally identified as a vasodilator, although it is now known to possess a variety of biological activities. Indicative of AM's novel angiogenic properties is our previous finding that *AM*$^{-/-}$ embryos die in utero due to hemorrhage and edema resulting from abnormalities of vascular development (14). We also showed previously that exogenous administration of AM enhances angiogenesis in ischemic tissues in adults, and therapeutic application of AM is much anticipated (25). Gene-targeted mice also provide information about the fundamental roles played by AM during the multistep process of angiogenesis. It is noteworthy, for instance, that *AM*$^{-/-}$ embryos die at a relatively late stage of development (E13.5–E14.5) compared with KO mice lacking other substances classified as angiogenic factors. This suggests that the vasculature does develop in *AM*$^{-/-}$ mice, but its fragile structure is likely disrupted after the start of circulation. It also clearly shows that AM is essential not only for angiogenesis, but also for vascular integrity.

As with other growth factors, the clinical applicability of AM has 2 serious limitations: AM is a peptide with a short half-life in the bloodstream, and the cost of the recombinant protein makes its use in the treatment of chronic diseases impractical. This prompted us to focus on AM's receptor system. McLatchie et al. showed that AM signaling is regulated by a unique control system (28). The main body of the AM receptor is thought to be CRLR, a 7-transmembrane domain GPCR. CRLR associates with 1 of 3 subtypes of RAMP, which determines the affinity of CRLR for its ligands. By generating RAMP2-specific KO mice, we have been able to demonstrate that RAMP2 is the key determinant of AM's function during vascular development. In our *RAMP2*$^{-/-}$ mice, CRLR and the other RAMPs were preserved; nevertheless, deletion of RAMP2 was sufficient to reproduce the phenotypes of the *AM*$^{-/-}$ genotype. Our finding that AM expression was upregulated in *RAMP2*$^{-/-}$ embryos just before their death further confirms that RAMP2 is essential for AM signaling during vascular development.

In both *AM*$^{-/-}$ and *RAMP2*$^{-/-}$ embryos, vascular fragility ultimately leads to hemorrhage and edema. Notably, however, the systemic edema was much more severe in *RAMP2*$^{-/-}$ mice. Edema was sometimes detected in *AM*$^{-/-}$ mice, but its severity varied. Moreover, administration of recombinant AM to crossbred *AM*$^{+/-}$ females increased the survival rate of *AM*$^{-/-}$ embryos at E14.5 (14), suggesting that maternally supplied AM partially compensates for the lack of embryonic AM expression. By contrast, *RAMP2*$^{-/-}$ mice cannot express a functional AM receptor in their vasculature and thus can not respond to maternal AM.

We found that neovascularization was diminished and vascular permeability was increased in adult *RAMP2*$^{+/-}$ mice, which showed reduced expression of RAMP2. We also found that *RAMP2*$^{+/-}$ mice had higher BP than did their WT littermates, which confirms that RAMP2 continues to be a crucial determinant of vascular function in the adult. Interestingly, we also found that the edema developed by *RAMP2*$^{+/-}$ mice in various disease models was more severe than that in WT mice, suggesting the AM-RAMP2 system could be an attractive therapeutic target for treating the edema often associated with vascular regenerative therapies, brain trauma, and infarction. In that regard, it is noteworthy that we were able to modulate the vascular function of AM by modulating RAMP2. Using RAMP2O/E cells, we clearly showed that by upregulating RAMP2 signaling, we could enhance capillary formation, firm up tight junctions, and reduce vascular permeability. RAMP2O/E cells were also resistant to apoptosis. Thus, RAMP2 could be a therapeutic target by which to manipulate the vascular functions of AM.

By contrast, RAMP3O/E cell lines did not show either enhanced angiogenesis or improved vascular stability, although RAMP3 has previously been shown to work with CRLR to function as another AM receptor (37). Furthermore, our finding that RAMP3 was expressed at WT levels in *RAMP2*$^{-/-}$ mice confirmed that RAMP3 cannot compensate for the absence of RAMP2 during vascular development. Consistent with the distinctly different physiologi-

cal roles played by RAMP2 and RAMP3, *RAMP3*$^{-/-}$ mice live apparently normally until old age (38). In addition, whereas RAMP2 and CRLR are downregulated in an endotoxemia model, RAMP3 is markedly upregulated (39), and it has been suggested that RAMP3 may be involved in post-endocytic receptor trafficking, as it presents a PDZ type I domain (40).

Signal transduction via GPCRs and the regulation of their function has long attracted the interest of many researchers. Indeed, about 40% of the drugs in clinical use today target GPCRs. We suggest that RAMP2 is an alternative therapeutic target by which to affect CRLR function. Because RAMP2 is a low-MW protein, structural analysis and the synthesis of specific agonists or antagonists are much more realistic for RAMP2 than for 7-transmembrane domain GPCRs, which has proven difficult. Moreover, because RAMP2 determines the vascular functions of AM, it would be expected that greater specificity would be achieved by targeting RAMP2 than by targeting CRLR, which can also function as a receptor for other ligands. In that context, our findings provide a clear basis for the development of drugs to modulate RAMP2 and, thereby, the vascular effects of AM.

Methods

Generation of RAMP2 KO mice. KO mice were generated as described previously (14, 16, 41, 42). Briefly, a plasmid-targeting vector was constructed to insert loxP sites encompassing exons 2–4 of *RAMP2* and the neomycin resistance gene, after which the plasmid was linearized and introduced into Bruce 4 embryonic stem cells by electroporation. Homologous recombinants were identified, and 2 independently targeted clones were injected into BALB/c blastocysts to generate chimeric mice. Male chimeras were crossbred with C57BL/6 females, and germline transmission was verified by Southern blot analysis. After obtaining heterozygotic floxed RAMP2 mice, we crossbred them with CAG-Cre mice to delete exons 2–4 of the *RAMP2* gene. The deletion of RAMP2 was certified by Southern blot analysis. The Cre gene was then removed from the line by backcrossing with C57BL/6 mice. All experiments were performed in accordance with the Declaration of Helsinki and were approved by the Shinshu University Ethics Committee for Animal Experiments.

In situ hybridization. In situ hybridization was performed as described previously (43). cRNAs were prepared from linearized cDNA templates of murine RAMP2 (ACACTTTGCGAACTGCTCCCTGGTGCAGCCCACCTTCTCTGATCCCCCAGAGGATGTGCTCCTGGCCATGATCATAGCCCCCATCTGCCTCATCCCGTTCCTTGTTACTCTTGTGGTGTGGAGGAGTAAAGACAGCGATGCCCAGGCCTAGGGTCCATTTCTCAGCAGCCATTTTTCCCCCCTTTTCCCTGCTGGAACCAGGAATGGCGCTCCTCCCCTCCCTACCCACTTACTCTCATCCTTCCCACAGACCTGTGGATTGGTGGAAATGGCAGCAAAGGGGACTCACGACACAATG) to generate antisense and sense probes. The cRNA transcripts were synthesized according to the manufacturer's instructions (Ambion).

Histological examination. Whole embryos, yolk sac and placenta, were fixed in 4% phosphate-buffered paraformaldehyde (pH 7.2), embedded in paraffin, and cut into 4-μm sections for histological examination. Some yolk sacs were used for immunohistochemical staining with anti-mouse CD31 antibody (BD Biosciences – Pharmingen) to visualize blood vessels. Samples were stained with a Histofine MOUSESTAIN KIT (Nichirei Biosciences) and DAB chromogen and counterstained with methyl green. Apoptosis was visualized in green fluorescence using the TUNEL method with an Apoptosis In Situ Detection Kit (Chemicon) and nuclei were stained with Hoechst 33342. To evaluate the aortic wall structure, immunohistochemical staining was performed using anti-mouse type IV collagen antibody (Collaborative Research), phalloidin, and DAPI (Roche Diagnostics). Confocal microscopic observation was then carried out using a Leica TCS-SP2 laser scanning microscope.

Transmission electron microscopy. Specimens were fixed in 2% glutaraldehyde (pH 7.2) and 4% osmium tetroxide, embedded in epoxy resin (Epok) 812 (Oken Shoji Co.), cut into ultrathin sections, double-stained with uranyl acetate and lead citrate, and examined by electron microscopy (JEM-1010; Jeol).

Quantitative real-time PCR analysis. Total RNA was extracted from tissues or cells using TRIzol Reagent (Invitrogen), after which it was treated with DNA-Free (Ambion) to remove contaminating DNA and subjected to reverse transcription using an Omniscript RT kit (QIAGEN) with random primers (Invitrogen). Quantitative real-time RT-PCR analysis was carried out using an ABI PRISM 7300 Sequence Detection System (Applied Biosystems) with SYBR Green (Toyobo) or TaqMan probe, and values were normalized to 18S rRNA (TaqMan Ribosomal RNA Control Reagents VIC Probe; Applied Biosystems). The primers and probes used were as follows: mouse AM (mAM) forward, 5′-CTACCGCCAGAGCATGAACC-3′; mAM reverse, 5′-GAAATGTGCAGGTCCCGAA-3′; mAM probe, 5′-CCCGCAGCAATGGATGCCG-3′; mRAMP2 forward, 5′-GCAGCCCACCTTCTCTGATC-3′; mRAMP2 reverse, 5′-AACGGGATGAGGCAGATGG-3′; mRAMP2 probe, 5′-CCCAGAGGATGTGCTCCTGGCCAT-3′; mRAMP3 forward, 5′-TGCAACGAGACAGGGATGC-3′; mRAMP3 reverse, 5′-GCATCATGTCAGCGAAGGC-3′; mRAMP3 probe, 5′-AGAGGCTGCCTCGCTGTGGGAA-3′; mCRLR forward, 5′-AGGCGTTTACCTGCACACACT-3′; mCRLR reverse, 5′-CAGGAAGCAGAGGAAACCCC-3′; mCRLR probe, 5′-ATCGTGGTGGCTGTGTTTGCGGAG-3′; mVE-cadherin forward: 5′-GGTGGCCAAAGACCCTGAC-3′; mVE-cadherin reverse, 5′-ACTGGTCTTGCGGATGGAGT-3′; mCDN5 forward, 5′-GCCTTCCTGGACCACAACA-3′; mCDN5 reverse, 5′-ACGACATCCACAGCCCCTT-3′; mCDN5 probe, 5′-CGTGACGGCGCAGACGACTTG-3′; mα2 type IV collagen forward, 5′-CACAACATCAACGATCCACCC-3′; mα2 type IV collagen reverse, 5′-GAACCCCATGATGCCTTCCT-3′; mα2 type IV collagen probe, 5′-AGCAAGGGATACCCGGCGTAATCTCA-3′; human VEGF (hVEGF) forward, 5′-TACCTCCACCATGCCAAGTG-3′; hVEGF reverse, 5′-GTGATGATTCTGCCCTCCTCC-3′; heNOS forward, 5′-AGATCTCCGCCTCGCTCAT-3′; heNOS reverse, 5′-AGCCATACAGGATTGTCGCC-3′; hCDN5 forward, 5′-AGGCGTGCTCTACCTGTTTTG-3′; hCDN5 reverse, 5′-AACTCGCGGACGACAATGTT-3′.

The PI3K inhibitor LY294002 (10^{-6} M) and a PKA inhibitor (14-22 cell permeable PKA inhibitor; 10^{-6} M) were obtained from Calbiochem.

Establishment of the RAMP2O/E line. The RAMP2O/E cell line was created using EAhy926 ECs, an immortal, clonally pure, human EC line obtained through hybridization of HUVECs and line A 549/8 lung carcinoma cells (kindly provided by C.J. Edgell, University of North Carolina, Chapel Hill, North Carolina, USA). EAhy926 human ECs were cultured in DMEM (Invitrogen) supplemented with 10% FBS (EQUITECH-BIO INC.). Full-length hRAMP2 cDNA was obtained from the UMR cDNA Resource Center (University of Missouri-Rolla). hRAMP2 (580 bp) labeled with HA-tag was inserted into the cloning site of pcDNA3.1$^+$ vector (Invitrogen), which was then linearized and transfected into EAhy926 cells using Effectene transfection reagent (QIAGEN). Four cell lines overexpressing RAMP2 were then cloned from G418-resistant (400 μg/ml) colonies. EAhy926 cells transfected with empty pcDNA3.1$^+$ vector served as controls.

Capillary formation on Matrigel. RAMP2O/E cells or control ECs were cultured on 24-well culture plates coated with Matrigel (BD) in medium containing 10^{-7} M recombinant hAM (Peptide Institute), and capillary formation was monitored microscopically. Photomicrographs were taken of 2 different fields in each well, and the degree of capillary formation was evaluated by quantification of the total capillary area in each field using

NIH Image software. Capillary area was then presented relative to the cell surface area of the control cells on day 1.

In vitro vascular permeability assay. To assay vascular permeability in vitro, we used a permeability chamber consisting of a 24-well tissue culture plate with cell culture inserts. The inserts contained a transparent polyethylene membrane with a high density of symmetrical pores (1 μm in diameter) that permitted high rates of basolateral diffusion. RAMP2O/E and control cells were seeded onto collagen-coated (Cellmatrix Type I-C; Nitta Gelatin Inc.) inserts, after which confluent endothelial monolayers that occluded the membrane pores were allowed to form over several days. The cell monolayers were then treated with 10 ng/ml VEGF, after which 13.3 mg/ml Dextran FITC Conjugate (MW 70,000; Research Organics) was added on top of the cells. The permeability of the monolayer was then assessed by measuring the fluorescence of the solution in the wells using a Multi-Detection Microplate Reader (POWERSCAN HT; DS Pharma Biomedical). The excitation and emission wavelengths were 485 nm and 530 nm, respectively.

Structure of tight junction after cell injury. EAhy926 ECs were cultured until confluent on chamber slides in DMEM containing 10^{-7} M AM and then exposed to 0.5 mM H_2O_2. Two hours after the H_2O_2 treatment, the cells were immunostained with anti-ZO-1 antibody (BD Biosciences – Pharmingen) and the nucleus-specific dye Hoechst 33342 (Sigma-Aldrich) and observed under a confocal microscope.

Aortic ring assay. After mice were killed with an overdose of anesthetic, the thoracic aorta was dissected from the posterior mediastinum, placed in serum-free EBM-2 endothelial basal medium (Cambrex), and cleaned of blood and fibroadipose tissue under a stereoscopic microscope using fine forceps and scissors. The vessel was then cut into 1-mm-long rings, which were subjected to 8 consecutive washes with serum-free EBM-2. The aortic rings were then embedded in thick collagen gel (Cellmatrix Type I-A; Nitta Gelatin Inc.) and cultured for 7 days, with or without recombinant hVEGF (50 ng/ml; R&D Systems) supplement. The capillaries that sprouted from the edges of the rings were analyzed (44).

Matrigel assay. After mice were anesthetized, 500 μl Matrigel (BD) containing 100 ng recombinant hbFGF (Wako) was injected subcutaneously into the dorsal region using a 25-gauge needle and permitted to solidify. Seven days later, the mice were killed with an overdose of anesthetic, the skin around the injected sites was incised, and the angiogenic response to the implanted Matrigel was analyzed.

AGM culture. Tissue culture of the AGM regions was carried out as described previously (45). The AGM regions were dissected from E10.5 embryos and plated on mouse OP9 stromal cells cultured on a 24-well dish. After 5 days of culture, capillaries growing from the AGM explant were stained with anti-CD31 antibody.

Footpad edema model. Vascular permeability leading to mouse footpad edema was assayed as described previously (46). Briefly, 20 μl of 0.01 g/ml λ-carrageenan (Wako) was injected subcutaneously into the footpads of 8-week-old mice, after which the swelling of the footpad was monitored using a thickness gauge (resolution, 1 μm).

Skin edema model. Vascular permeability leading to mouse skin edema was assayed as described previously (47). Mice were injected via the tail vein with 0.2 ml of 1.5% FITC-BSA (15 mg/ml) in isotonic Tyrode solution, which served as a tracer of vascular permeability. Thereafter, serum exudation was induced by subcutaneous injection of histamine (1 μg/100 μl/site) into the shaved dorsal skin. Thirty minutes later, the injected sites in the dorsal skin were removed as circular patches and put into the wells of a 24-well culture plate. Formamide (1 ml) was then added to each well and incubated at 50°C for 2 h, after which the fluorescence intensity in each well was measured using a Multi-Detection Microplate Reader; the excitation and emission wavelengths were 485 nm and 530 nm, respectively.

Brain edema model (cold lesion model). Mice were mounted in a stereotaxic frame (Narishige), after which the scalp was incised, subcutaneous tissue was retracted from the bone, and the skull was exposed. Using a drill, a circular craniotomy was then carried out over the right parietal cortex, extending from the lambda suture to bregma, and the resultant bone flap was lifted off to expose the underlying dura. The cold lesion was made using a copper cylinder (3 mm in diameter) that had been precooled with liquid nitrogen. The metal probe was lowered quickly onto the surface of the intact dura over the parietotemporal cortex under microscopic control and pressed down to a depth of 1 mm for 30 seconds (48).

To quantify the vascular permeability of brain vessels, 0.2 ml of sodium fluorescein at a concentration of 6 mg/ml in PBS was injected via the tail vein 24 hours after making the cold lesions. Thirty minutes later, the mice were anesthetized and perfused with PBS (20 ml) via the left cardiac ventricle to remove the fluorescent tracer from the vascular bed. To assess their fluorescence, brain hemispheres were homogenized in 0.5 M borate buffer (pH 10) and centrifuged (800 *g*) for 15 min at 4°C, after which the supernatant was added to 1.2 ml of ethanol to precipitate the proteins. The samples were again centrifuged, and the fluorescence in the supernatant was measured using a Multi-Detection Microplate Reader (49); the excitation and emission wavelengths were 330 nm and 485 nm, respectively.

Statistics. Quantitative values are expressed as mean ± SE. Student's *t* tests were used to determine significant differences. Values of $P < 0.05$ were considered significant.

Acknowledgments

We thank C.J. Edgell for EAhy926 cells. This study was supported by a grant from the Takeda Medical Research Foundation; a Japan Heart Foundation Research Grant; a Grant for Research on Cardiovascular Disease from the Tanabe Medical Conference; a grant from the Novartis Foundation for Gerontological Research; an Astra Zeneca Research Grant; grants from the Mitsui Life Social Welfare Foundation, the Ichiro Kanehara Foundation, the Uehara Memorial Foundation, the Sankyo Foundation of Life Science, the Naito Foundation, the Mitsubishi Pharma Research Foundation, and the Salt Science Research Foundation; Research Grant for Cardiovascular Disease 19C-7 from the Ministry of Heath, Labour and Welfare; and a Grant-in-Aid for Scientific Research from the Ministry of Education, Culture, Sports, Science and Technology, Japan.

Received for publication June 18, 2007, and accepted in revised form November 7, 2007.

Address correspondence to: Takayuki Shindo, Department of Organ Regeneration, Shinshu University Graduate School of Medicine, 3-1-1 Asahi, Matsumoto 390-8621, Japan. Phone: 81-263-37-3192; Fax: 81-263-37-3437; E-mail: t-shindo@sch.md.shinshu-u.ac.jp.

1. Kitamura, K., et al. 1993. Adrenomedullin: a novel hypotensive peptide isolated from human pheochromocytoma. *Biochem. Biophys. Res. Commun.* **192**:553–560.
2. Michibata, H., et al. 1998. Autocrine/paracrine role of adrenomedullin in cultured endothelial and mesangial cells. *Kidney Int.* **53**:979–985.
3. Kitamura, K., et al. 1994. Immunoreactive adrenomedullin in human plasma. *FEBS Lett.* **341**:288–290.
4. Jougasaki, M., et al. 1995. Renal localization and actions of adrenomedullin: a natriuretic peptide. *Am. J. Physiol.* **268**:F657–F663.
5. Nishikimi, T., and Matsuoka, H. 2005. Cardiac adrenomedullin: its role in cardiac hypertrophy and heart failure. *Curr. Med. Chem. Cardiovasc. Hematol. Agents.* **3**:231–242.
6. Samson, W.K., Murphy, T., and Schell, D.A. 1995. A novel vasoactive peptide, adrenomedullin, inhibits pituitary adrenocorticotropin release. *Endocrinology.* **136**:2349–2352.
7. Petrie, M.C., Hillier, C., Morton, J.J., and McMurray, J.J. 2000. Adrenomedullin selectively inhibits angiotensin II-induced aldosterone secretion in

humans. *J. Hypertens.* **18**:61–64.
8. Isumi, Y., Kubo, A., Katafuchi, T., Kangawa, K., and Minamino, N. 1999. Adrenomedullin suppresses interleukin-1beta-induced tumor necrosis factor-alpha production in Swiss 3T3 cells. *FEBS Lett.* **463**:110–114.
9. Shimosawa, T., et al. 2002. Adrenomedullin, an endogenous peptide, counteracts cardiovascular damage. *Circulation.* **105**:106–111.
10. Shimosawa, T., et al. 2003. Deficiency of adrenomedullin induces insulin resistance by increasing oxidative stress. *Hypertension.* **41**:1080–1085.
11. Kano, H., et al. 1996. Adrenomedullin as a novel antiproliferative factor of vascular smooth muscle cells. *J. Hypertens.* **14**:209–213.
12. Miyashita, K., et al. 2003. Adrenomedullin promotes proliferation and migration of cultured endothelial cells. *Hypertens. Res.* **26**(Suppl.):S93–S98.
13. Iwasaki, H., Eguchi, S., Shichiri, M., Marumo, F., and Hirata, Y. 1998. Adrenomedullin as a novel growth-promoting factor for cultured vascular smooth muscle cells: role of tyrosine kinase-mediated mitogen-activated protein kinase activation. *Endocrinology.* **139**:3432–3441.
14. Shindo, T., et al. 2001. Vascular abnormalities and elevated blood pressure in mice lacking adrenomedullin gene. *Circulation.* **104**:1964–1971.
15. Shindo, T., et al. 2000. Hypotension and resistance to lipopolysaccharide-induced shock in transgenic mice overexpressing adrenomedullin in their vasculature. *Circulation.* **101**:2309–2316.
16. Oh-hashi, Y., et al. 2001. Elevated sympathetic nervous activity in mice deficient in alphaCGRP. *Circ. Res.* **89**:983–990.
17. Niu, P., et al. 2004. Protective effects of endogenous adrenomedullin on cardiac hypertrophy, fibrosis, and renal damage. *Circulation.* **109**:1789–1794.
18. Niu, P., et al. 2003. Accelerated cardiac hypertrophy and renal damage induced by angiotensin II in adrenomedullin knockout mice. *Hypertens. Res.* **26**:731–736.
19. Nishimatsu, H., et al. 2002. Role of endogenous adrenomedullin in the regulation of vascular tone and ischemic renal injury: studies on transgenic/knockout mice of adrenomedullin gene. *Circ. Res.* **90**:657–663.
20. Imai, Y., et al. 2002. Resistance to neointimal hyperplasia and fatty streak formation in mice with adrenomedullin overexpression. *Arterioscler. Thromb. Vasc. Biol.* **22**:1310–1315.
21. Yamamoto, H., et al. 2007. Adrenomedullin insufficiency increases allergen-induced airway hyperresponsiveness in mice. *J. Appl. Physiol.* **102**:2361–2368.
22. Kurihara, H., Shindo, T., Oh-Hashi, Y., Kurihar, Y., and Kuwaki, T. 2003. Targeted disruption of adrenomedullin and alphaCGRP genes reveals their distinct biological roles. *Hypertens. Res.* **26**(Suppl.):S105–S108.
23. Nishimatsu, H., et al. 2003. Endothelial responses of the aorta from adrenomedullin transgenic mice and knockout mice. *Hypertens. Res.* **26**(Suppl.):S79–S84.
24. Aoki-Nagase, T., et al. 2002. Attenuation of antigen-induced airway hyperresponsiveness in CGRP-deficient mice. *Am. J. Physiol. Lung Cell Mol. Physiol.* **283**:L963–L970.
25. Iimuro, S., et al. 2004. Angiogenic effects of adrenomedullin in ischemia and tumor growth. *Circ. Res.* **95**:415–423.
26. Fujii, T., et al. 2005. Adrenomedullin enhances therapeutic potency of bone marrow transplantation for myocardial infarction in rats. *Am. J. Physiol. Heart Circ. Physiol.* **288**:H1444–H1450.
27. Nagaya, N., et al. 2005. Adrenomedullin: angiogenesis and gene therapy. *Am. J. Physiol. Regul. Integr. Comp. Physiol.* **288**:R1432–R1437.
28. McLatchie, L.M., et al. 1998. RAMPs regulate the transport and ligand specificity of the calcitonin-receptor-like receptor. *Nature.* **393**:333–339.
29. Kuwasako, K., Cao, Y.N., Nagoshi, Y., Kitamura, K., and Eto, T. 2004. Adrenomedullin receptors: pharmacological features and possible pathophysiological roles. *Peptides.* **25**:2003–2012.
30. Parameswaran, N., and Spielman, W.S. 2006. RAMPs: The past, present and future. *Trends Biochem. Sci.* **31**:631–638.
31. Morfis, M., Christopoulos, A., and Sexton, P.M. 2003. RAMPs: 5 years on, where to now? *Trends Pharmacol. Sci.* **24**:596–601.
32. Montuenga, L.M., Martinez, A., Miller, M.J., Unsworth, E.J., and Cuttitta, F. 1997. Expression of adrenomedullin and its receptor during embryogenesis suggests autocrine or paracrine modes of action. *Endocrinology.* **138**:440–451.
33. Montuenga, L.M., Mariano, J.M., Prentice, M.A., Cuttitta, F., and Jakowlew, S.B. 1998. Coordinate expression of transforming growth factor-beta1 and adrenomedullin in rodent embryogenesis. *Endocrinology.* **139**:3946–3957.
34. Bauer, J., et al. 1992. In vitro model of angiogenesis using a human endothelium-derived permanent cell line: contributions of induced gene expression, G-proteins, and integrins. *J. Cell Physiol.* **153**:437–449.
35. Edgell, C.J., Curiel, D.T., Hu, P.C., and Marr, H.S. 1998. Efficient gene transfer to human endothelial cells using DNA complexed to adenovirus particles. *Biotechniques.* **25**:264–268, 270–272.
36. Lee, R.J., et al. 2000. VEGF gene delivery to myocardium: deleterious effects of unregulated expression. *Circulation.* **102**:898–901.
37. Sexton, P.M., Albiston, A., Morfis, M., and Tilakaratne, N. 2001. Receptor activity modifying proteins. *Cell Signal.* **13**:73–83.
38. Dackor, R.T., Fritz-Six, K.L., Smithies, O., and Caron, K.M. 2007. Receptor activity modifying proteins 2 and 3 have distinct physiological functions from embryogenesis to old age. *J. Biol. Chem.* **282**:18094–18099.
39. Ono, Y., Okano, I., Kojima, M., Okada, K., and Kangawa, K. 2000. Decreased gene expression of adrenomedullin receptor in mouse lungs during sepsis. *Biochem. Biophys. Res. Commun.* **271**:197–202.
40. Bomberger, J.M., Parameswaran, N., Hall, C.S., Aiyar, N., and Spielman, W.S. 2005. Novel function for receptor activity-modifying proteins (RAMPs) in post-endocytic receptor trafficking. *J. Biol. Chem.* **280**:9297–9307.
41. Shindo, T., et al. 2000. ADAMTS-1: a metalloproteinase-disintegrin essential for normal growth, fertility, and organ morphology and function. *J. Clin. Invest.* **105**:1345–1352.
42. Shindo, T., et al. 2002. Kruppel-like zinc-finger transcription factor KLF5/BTEB2 is a target for angiotensin II signaling and an essential regulator of cardiovascular remodeling. *Nat. Med.* **8**:856–863.
43. Lyons, G.E., Schiaffino, S., Sassoon, D., Barton, P., and Buckingham, M. 1990. Developmental regulation of myosin gene expression in mouse cardiac muscle. *J. Cell Biol.* **111**:2427–2436.
44. Zhu, W.H., Iurlaro, M., MacIntyre, A., Fogel, E., and Nicosia, R.F. 2003. The mouse aorta model: influence of genetic background and aging on bFGF- and VEGF-induced angiogenic sprouting. *Angiogenesis.* **6**:193–199.
45. Hamaguchi, I., et al. 1999. In vitro hematopoietic and endothelial cell development from cells expressing TEK receptor in murine aorta-gonad-mesonephros region. *Blood.* **93**:1549–1556.
46. Sakurai, K., et al. 1997. Anti-inflammatory activity of superoxide dismutase conjugated with sodium hyaluronate. *Glycoconj. J.* **14**:723–728.
47. Yamaki, K., Takano-Ishikawa, Y., Goto, M., Kobori, M., and Tsushida, T. 2002. An improved method for measuring vascular permeability in rat and mouse skin. *J. Pharmacol. Toxicol. Methods.* **48**:81–86.
48. Hortobagyi, T., et al. 2000. A novel brain trauma model in the mouse: effects of dexamethasone treatment. *Pflugers Arch.* **441**:409–415.
49. Schoch, H.J., Fischer, S., and Marti, H.H. 2002. Hypoxia-induced vascular endothelial growth factor expression causes vascular leakage in the brain. *Brain.* **125**:2549–2557.

Single Injection of a Sustained-release Prostacyclin Analog Improves Pulmonary Hypertension in Rats

Hiroaki Obata[1,2], Yoshiki Sakai[3], Shunsuke Ohnishi[1], Satoshi Takeshita[4], Hidezo Mori[5], Makoto Kodama[2], Kenji Kangawa[6], Yoshifusa Aizawa[2], and Noritoshi Nagaya[1,4]

[1]Department of Regenerative Medicine and Tissue Engineering, National Cardiovascular Center Research Institute, Osaka, Japan; [2]Division of Cardiology, Niigata University Graduate School of Medical and Dental Science, Niigata, Japan; [3]Ono Pharmaceutical Co. Ltd., Research Headquarters, Osaka, Japan; [4]Department of Internal Medicine, National Cardiovascular Center, Osaka, Japan; [5]Department of Cardiac Physiology, National Cardiovascular Center Research Institute, Osaka, Japan; and [6]Department of Biochemistry, National Cardiovascular Center Research Institute, Osaka, Japan

Rationale: Although prostacyclin is recognized as a therapeutic breakthrough for pulmonary hypertension, it needs continuous infusion because of its short action. Therefore, we developed a new drug delivery system for prostacyclin. We prepared ONO-1301MS, a novel sustained-release prostacyclin analog polymerized with poly(D, L-lactic-co-glycolic acid) (PLGA) microspheres.

Objectives: We examined whether ONO-1301MS attenuates monocrotaline (MCT)-induced pulmonary hypertension in rats, and attempted to elucidate the underlying mechanisms responsible for the beneficial effects of ONO-1301MS.

Methods: After MCT injection, rats were randomized to receive a single subcutaneous injection of 100 mg/kg ONO-1301MS or vehicle.

Measurements and Main Results: We prepared ONO-1301MS, which was polymerized with PLGA to release ONO-1301 for 3 weeks. A single administration of ONO-1301MS achieved sustained elevation of its circulating level and plasma cyclic adenosine 3',5'-monophosphate level for 3 weeks, and attenuated an increase in a metabolite of thromboxane A_2 level. Rats had developed pulmonary hypertension 3 weeks after MCT injection; however, treatment with ONO-1301MS significantly attenuated the increases in right ventricular systolic pressure and right ventricular weight to body weight ratio. ONO-1301MS significantly inhibited hypertrophy of pulmonary arteries. Phosphorylation of extracellular signal-regulated protein kinase (ERK) in the lung was significantly increased in the control group, whereas this increase was markedly attenuated by treatment.

Conclusions: We developed a new drug delivery system for prostacyclin using PLGA and ONO-1301. A single injection of ONO-1301MS resulted in sustained activity for 3 weeks, and attenuated pulmonary hypertension, partly through its antiproliferative effect on vascular smooth muscle cells via inhibition of ERK phosphorylation.

Keywords: pulmonary hypertension; prostacyclin analog; sustained-release preparation; extracellular signal regulated kinase; poly(lactic-co-glycolic acid)

AT A GLANCE COMMENTARY

Scientific Knowledge on the Subject

Although prostacyclin is recognized as a therapeutic breakthrough for pulmonary hypertension, it needs continuous infusion because of its short action. For patients with pulmonary hypertension, development of a sustained-release prostacyclin would be beneficial in terms of stable hemodynamics and quality of life.

What This Study Adds to the Field

A single injection of ONO-1301MS resulted in sustained activity for 3 weeks, and attenuated pulmonary hypertension in rats.

Pulmonary arterial hypertension is a rare but life-threatening disease characterized by progressive pulmonary hypertension that leads to right ventricular (RV) failure and death (1). Prostacyclin, a metabolite of arachidonic acid, has vasoprotective effects, including vasodilation, antiplatelet aggregation, and inhibition of smooth muscle cell (SMC) proliferation (2–4). Thus, continuous intravenous infusion of prostacyclin (epoprostenol) has become recognized as a therapeutic breakthrough for pulmonary arterial hypertension (5–7). The dramatic success of long-term intravenous prostacyclin has led to the development of prostacyclin analogs (8–11). Nevertheless, treatment with prostacyclin or its analogs has some problems in the clinical setting. Epoprostenol therapy requires a continuous intravenous infusion device, and is therefore more invasive and uncomfortable than taking prostacyclin analogs. On the other hand, prostacyclin analogs, such as subcutaneously infused treprostinil, inhaled iloprost, and oral beraprost, need continuous infusion or frequent administration because of their short duration of action (5–11). In fact, epoprostenol has a very short half-life (<6 min) (12), treprostinil has been reported to have a half-life of 4.6 hours after cessation of continuous subcutaneous infusion (13), iloprost has a serum half-life of 20 to 25 minutes, and the elimination half-life of beraprost is 35 to 40 minutes after oral administration (12).

Recently, we developed a new type of prostacyclin agonist, ONO-1301 (Figure 1), which has long-lasting prostacyclin activity and an inhibitory effect on thromboxane synthase (14). ONO-1301 does not contain prostanoid structures, such as a five-membered ring or allylic alcohol, which are digested by 15-hydroxyprostaglandin dehydrogenase (Figure 1). These structures are considered to be crucial for the stable activity of ONO-1301. This agent is metabolized by cytochrome P450, and the half-life was about 5.6 hours in our previous study (14). In

(Received in original form March 1, 2007; accepted in final form October 26, 2007)

Supported by research grants from Ono Pharmaceutical Co., Ltd. (no. 526); Human Genome Tissue Engineering 009 from the Ministry of Health, Labor, and Welfare; the Program for Promotion of Fundamental Studies in Health Science of the National Institute of Biomedical Innovation (NIBIO); and a Grant-in-Aid for Exploratory Research from the Ministry of Education, Culture, Sports, Science, and Technology.

Correspondence and requests for reprints should be addressed to Noritoshi Nagaya, M.D., Department of Regenerative Medicine and Tissue Engineering, National Cardiovascular Center Research Institute, 5-7-1 Fujishirodai, Suita, Osaka 565-8565, Japan. E-mail: nnagaya@ri.ncvc.go.jp

This article contains an online supplement, which is accessible from this issue's table of contents at www.atsjournals.org

Am J Respir Crit Care Med Vol 177. pp 195–201, 2008
Originally Published in Press as DOI: 10.1164/rccm.200703-349OC on November 1, 2007
Internet address: www.atsjournals.org

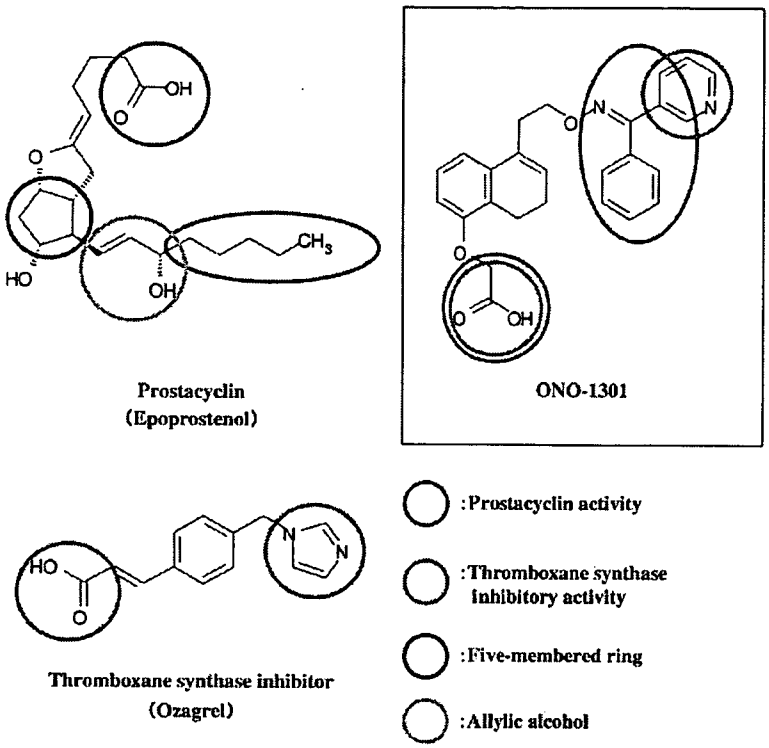

Figure 1. Chemical structures of ONO-1301, epoprostenol (prostacyclin analog), and ozagrel (thromboxane synthase inhibitor). Epoprostenol shares common characteristics with prostanoid structures, including a five-membered ring and an allylic alcohol (*blue* and *yellow circles*, respectively). In contrast, ONO-1301 has a carboxylic acid and a lipid-soluble functional group that activates the prostacyclin receptor (*green circles*), but does not have prostanoid structures, which allow long-lasting prostacyclin activity. Unlike epoprostenol, ONO-1301 has thromboxane synthase inhibitory activity because of a 3-pyridine radical and carboxylic acid within its molecule (*red circles*), similar to ozagrel.

addition, ONO-1301 has a 3-pyridine radical, which is known to inhibit thromboxane synthase through interaction with carboxylic acid via a hydrogen bond (Figure 1). Repeated administration of ONO-1301 attenuated monocrotaline (MCT)-induced pulmonary hypertension and improved survival in rats. Although the half-life of plasma ONO-1301 concentration is longer than that of any other prostacyclin analogs, ONO-1301 still needs to be administered twice a day subcutaneously to achieve a significant improvement in pulmonary hypertension. For patients with pulmonary hypertension, development of a long-acting, sustained-release prostacyclin analog would be beneficial in terms of stable hemodynamics and quality of life. To overcome these problems, we developed a new drug delivery system for prostacyclin. We prepared a novel sustained-release prostacyclin analog polymerized with poly(D,L-lactic-co-glycolic acid) (PLGA) microspheres (ONO-1301MS). PLGA microspheres, which are biodegradable and biocompatible compounds, have been used as a controlled delivery system for proteins and drugs (15–20). The release of drug from PLGA microspheres occurs through degradation of the polymeric matrix. Here, we showed that a single subcutaneous administration of ONO-1301MS achieved sustained elevation of its circulating level for 3 weeks.

Thus, the purposes of this study were as follows: (*1*) to investigate whether a single subcutaneous administration of ONO-1301MS attenuates MCT-induced pulmonary hypertension in rats and (*2*) to elucidate the underlying mechanisms responsible for the beneficial effects of this compound.

METHODS

Preparation of ONO-1301MS

ONO-1301MS is polymerized ONO-1301 with PLGA microspheres. ONO-1301 and PLGA (polylactic acid to glycolic acid ratio of 50:50) were dissolved in dichloromethane. The dissolved polymer was added to polyvinyl alcohol aqueous solution to form an oil-in-water emulsion. Then, dichloromethane was evaporated by stirring. After centrifugation and washing, ONO-1301MS was isolated by lyophilization.

Morphologic Studies by Scanning Electron Microscopy

To evaluate the shape and surface morphology of ONO-1301MS, we used a scanning electron microscope (model S-2460N; Hitachi, Tokyo, Japan). After lyophilization, the microspheres were mounted on an aluminum stub and coated with a thin layer (200 Å) of gold by an ion sputter (model E-1010; Hitachi). The surface morphology of the microsphere samples was then visualized under a scanning electron microscope.

Particle Diameter

ONO-1301MS was suspended in distilled water and dispersed by sonication. The particle diameter was measured by a laser diffraction particle size analyzer (model SALD-2100; Shimadzu, Kyoto, Japan).

Encapsulation Efficiency

Acetonitrile containing n-propyl 4-hydroxybenzoate served as an internal control to obtain the encapsulation efficiency, and this solution was homogenized by a sonicator. The concentration of ONO-1301 in this solution was analyzed by high-performance liquid chromatography (HPLC). The encapsulation efficiency was calculated as follows:

$$\text{Encapsulation efficiency}(\%) = (\text{measured value}/\text{theoretical value}) \times 100.$$

In Vitro Release of ONO-1301 from PLGA Microspheres

ONO-1301MS was suspended in phosphate-buffered saline (0.067 mol/L salt concentration, pH 6.8) containing 0.2% Tween-80 to adjust the concentration of ONO-1301 to 100 μg/ml. This solution was aliquoted into 1 ml and incubated at 37°C. At various time intervals, one of the aliquots was centrifuged for 5 minutes at 12,000 rpm. The supernatant was discarded, the pellet was dissolved in acetonitrile, and the remaining amount of ONO-1301 was analyzed by HPLC.

Animal Models

We used 5-week-old male Wistar rats weighing 95 to 110 g. The rats were randomly given a subcutaneous injection of either 60 mg/kg MCT or 0.9% saline, and assigned to receive a subcutaneous injection of 100 mg/kg ONO-1301MS or 0.9% saline. This protocol resulted in the creation of three groups: normal rats given 0.9% saline (sham group, n = 10), MCT rats given 0.9% saline (control group, n = 11), and MCT rats treated with ONO-1301 MS (treated group, n = 11). We chose the maximum dose that did not induce significant hypotension (*see* Figure E1 in the online supplement).

In Vivo Experimental Protocol

After anesthetization by an intraperitoneal injection of 30 mg/kg pentobarbital, rats were given a subcutaneous injection of either 60 mg/kg MCT or 0.9% saline. Subsequently, rats received a single subcutaneous injection of 100 mg/kg ONO-1301MS or 0.9% saline. ONO-1301MS was suspended with 0.9% saline containing 0.2% Tween-80. Hemodynamic measurements and histologic analyses were performed on Day 21. For hemodynamic measurements, rats were anesthetized by intraperitoneal injection of 20 mg/kg pentobarbital, and the following indexes were recorded after an equilibration period. A polyethylene catheter (model PE-50; BD Biosciences, San Jose, CA) was inserted into the right carotid artery to measure heart rate and mean arterial pressure. The catheter was inserted through the right jugular vein into the right ventricle for the measurement of RV pressure. The values of heart rate, mean arterial pressure, and systolic RV pressure were calculated from a series of 20 consecutive heart beats in each rat. Finally, cardiac arrest was induced by injection of 2 mmol/L potassium chloride through the catheter. The ventricles and lungs were excised, dissected free, and weighed. The RV weight to body weight ratio (RV/BW), left ventricular plus septal weight to body weight ratio (LV + S/BW), and RV weight to left ventricular plus septal weight ratio (RV/LV + S) were calculated as indexes of ventricular hypertrophy, as reported previously (21). All protocols were performed in accordance with the guidelines of the Animal Care Ethics Committee of the National Cardiovascular Center Research Institute (Osaka, Japan).

Morphometric Analysis of Pulmonary Arteries

Paraffin sections of 4-μm thickness were obtained from the lower region of the right lung and stained with hematoxylin and eosin. Analysis of the medial wall thickness of the pulmonary arteries was performed as described previously (22). In brief, the external diameter and the medial wall thickness were measured in 20 muscular arteries (25–100-μm external diameter) per lung section. For each artery, the medial wall thickness was expressed as follows:

$$\%\ \text{wall thickness} = ([\text{medial thickness} \times 2]/\text{external diameter}) \times 100$$

A lung section was obtained from individual rats for comparison among the three groups (n = 5 in each group).

Assay of Plasma Levels of ONO-1301 and Cyclic AMP

To investigate whether a single subcutaneous administration of ONO-1301MS produces long-lasting prostacyclin activity in rats, we measured plasma levels of ONO-1301 and cyclic AMP (cAMP) after ONO-1301MS injection. Fourteen rats were assigned to receive a single subcutaneous injection of 100 mg/kg ONO-1301MS or 0.9% saline (n = 7 in each group), and blood was drawn from the tail vein on Days 0, 7, 14, and 21. Blood was immediately transferred to a chilled glass tube containing 1 mg/ml disodium ethylenediaminetetraacetic acid and 500 U/ml aprotinin, and centrifuged immediately. Plasma ONO-1301 level was measured by liquid chromatography tandem mass spectrometry assay. Plasma cAMP level was measured with a radioimmunoassay kit (cAMP assay kit; Yamasa Co., Chiba, Japan), as reported previously (23).

Assay of Urinary Level of 11-Dehydro Thromboxane B_2

To investigate the effect of ONO-1301MS on thromboxane synthesis in rats, we measured urinary level of 11-dehydro thromboxane B_2 (11-DTXB$_2$), a metabolite of thromboxane A_2 (TXA$_2$), after single subcutaneous injection of ONO-1301MS (100 mg/kg) or vehicle (n = 8 in each group). Urine samples were collected for 24 hours on Day 14 by using metabolic cages, and urinary concentration of 11-DTXB$_2$ was measured with an enzyme immunoassay kit (11-DTXB$_2$ assay kit; Cayman Chemical Co., Ann Arbor, MI). The urinary level of 11-DTXB$_2$ was expressed as the ratio of urinary 11-DTXB$_2$ concentration to that of creatinine, as reported previously (24).

Western Blot Analysis

To investigate the effect of ONO-1301MS on proliferative signaling pathways in homogenized lung tissue, the protein expression of extracellular signal-regulated protein kinase (ERK) 1/2 and phospho-ERK1/2 was determined by Western blotting. Western blotting was performed using rabbit monoclonal antibodies raised against ERK1/2 and phospho-ERK1/2 (Cell Signaling Technology, Danvers, MA). Peripheral samples of lung tissue were obtained on Day 21 from individual rats for comparison among the three groups (n = 6 in each group). Positive protein bands were visualized by means of chemiluminescence (enhanced chemiluminescence kit; Amersham Biosciences, Little Chalfont, UK). Western blot analysis using a mouse polyclonal antibody raised against β-actin (Sigma Chemical Corp., St. Louis, MO) was used as a protein loading control. The resultant bands were quantified using Image J 1.36 imaging software (National Institutes of Health; http://rsb.info.nih.gov/ij/).

Statistical Analysis

All data were expressed as mean ± SEM. Comparisons of parameters among the three groups were made by one-way analysis of variance (ANOVA), followed by Newman-Keuls test. Comparisons of the time course of parameters between the two groups were made by two-way ANOVA for repeated measures, followed by Newman-Keuls test. A value of $P < 0.05$ was considered statistically significant.

RESULTS

Characterization of ONO-1301MS

We prepared three kinds of ONO-1301MS (samples 1, 2, and 3). The external surface morphology of ONO-1301MS (sample 2 as a representative sample) exhibited a spherical shape with a smooth and uniform surface (Figure 2A). The particle size in samples 1, 2, and 3 was 21.2, 42.0, and 71.1 μm, respectively (Figure 2B; sample 2 as a representative sample). Encapsulation efficiency in each sample was 5.1, 21.8, and 17.4%, respectively. *In vitro*, each sample had different time periods of ONO-1301 release at 2, 3, and 4 weeks, respectively (Figure 2C). These data suggest that we were able to vary the release period of ONO-1301.

Long-lasting Activity of ONO-1301MS

To investigate the pharmacokinetics *in vivo*, we measured plasma ONO-1301 level after a single subcutaneous administration of ONO-1301MS, which was designed to release ONO-1301 for 3 weeks (sample 2). ONO-1301 was detected in plasma for 3 weeks, whereas plasma ONO-1301 level at baseline in the ONO-1301MS group and at all times in the vehicle group was below the detection limit (Figure 3A). In addition, plasma cAMP level after a single subcutaneous administration of ONO-1301MS was significantly higher than that in the control group (Figure 3B). Interestingly, the increase in plasma cAMP level lasted for over 2 weeks in parallel with the change in plasma ONO-1301MS level (Figure 3). These results suggest that subcutaneous administration of ONO-1301MS achieves long-lasting activity in rats.

Inhibitory Effect of ONO-1301MS on Thromboxane Synthase

Urinary level of 11-DTXB$_2$ was markedly elevated 14 days after MCT injection (Figure 4). However, treatment with ONO-1301MS significantly decreased urinary level of 11-DTXB$_2$ in MCT rats. These results suggest that ONO-1301MS has a sustained inhibitory effect on thromboxane synthase activity.

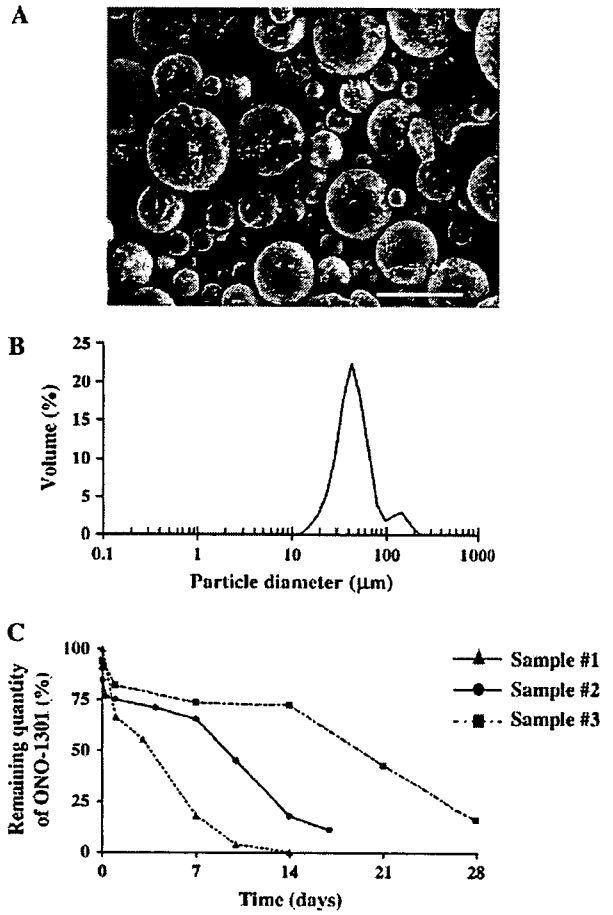

Figure 2. Physicochemical characteristics and *in vitro* release of ONO-1301. (*A*) Morphology of ONO-1301MS (sample 2) studied by scanning electron microscopy. *Scale bar* = 50 μm. (*B*) Particle diameter of ONO-1301MS (sample 2) obtained by a laser diffraction particle size analyzer. (*C*) Release profiles of ONO-1301MS in each sample.

Effects of ONO-1301MS on Pulmonary Hemodynamics and Vascular Remodeling

Three weeks after MCT injection, RV systolic pressure was markedly increased (Figure 5). However, the increase in RV systolic pressure was significantly attenuated in the treated group. Similarly, the increases in RV/BW and RV/LV + S in MCT rats were significantly attenuated by treatment with ONO-1301MS (Figure 5). There were no significant differences in heart rate or mean arterial pressure among the three groups (Table 1). Histologic examination demonstrated that hypertrophy of the pulmonary vascular wall was attenuated in the treated group compared with that in the control group (Figure 6).

No adverse reactions, such as flushing, diarrhea, or hypotension, were observed in the treated group, and there were no significant differences in blood biochemical markers of liver and renal function among the three groups (mean value ± SEM in sham, control, and treated group were, respectively: 139 ± 14, 145 ± 20, and 102 ± 12 IU/L in aspartate aminotransferase; 53 ± 3, 54 ± 5, and 45 ± 3 IU/L in alanine aminotransferase; 0.1 ± 0, 0.1 ± 0, and 0.1 ± 0 mg/dl in total bilirubin; 16.2 ± 1.1, 16.2 ± 0.4, and 15.4 ± 1.2 mg/dl in urea nitrogen; 0.22 ± 0.01, 0.21 ± 0.01, and 0.21 ± 0.01 mg/dl in creatinine; n = 5 in each group.). Moreover, no abnormality was observed at the injection site.

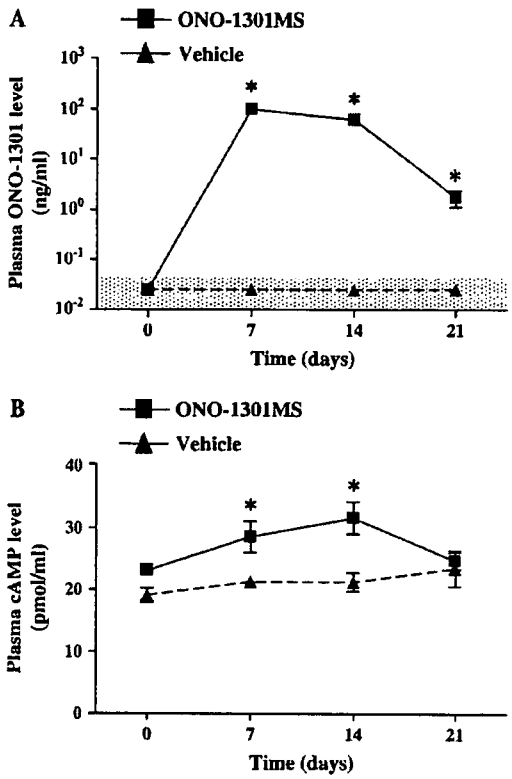

Figure 3. Time course changes in plasma ONO-1301 and cAMP. (*A*) Plasma ONO-1301 concentration after a single subcutaneous administration of ONO-1301MS or vehicle. The *shaded area* indicates below the lower limit of quantification (0.025 ng/ml) and is treated as 0 in the statistical analysis. (*B*) Changes in plasma cAMP level after a single subcutaneous administration of ONO-1301 MS or vehicle. Data are mean ± SEM. *$P < 0.05$ versus vehicle.

Inhibitory Effect of ONO1301-MS on Proliferative Signals

To investigate the effect of ONO1301-MS on proliferative signals in the lung, Western blot analyses were performed. There were no significant differences in the expression of ERK1 and ERK2 among the three groups (Figure 7). However, phosphorylation of ERK1 and ERK2 was significantly increased in the control group, whereas these increases were markedly attenuated in the treatment group (Figure 7).

DISCUSSION

In the present study, we demonstrated that (*1*) a novel sustained-release prostacyclin analog polymerized with PLGA

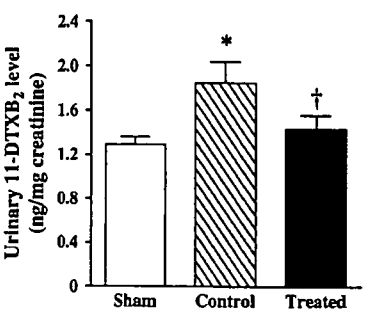

Figure 4. Effect of ONO-1301MS on thromboxane synthesis. Changes in urinary 11-dehydro thromboxane B_2 (11-DTXB_2) level on Day 14. Sham = sham rats given vehicle; control = monocrotaline (MCT)-treated rats given vehicle; treated = MCT rats treated with ONO-1301MS. Data are mean ± SEM. *$P <$ 0.05 versus sham; †$P <$ 0.05 versus control.

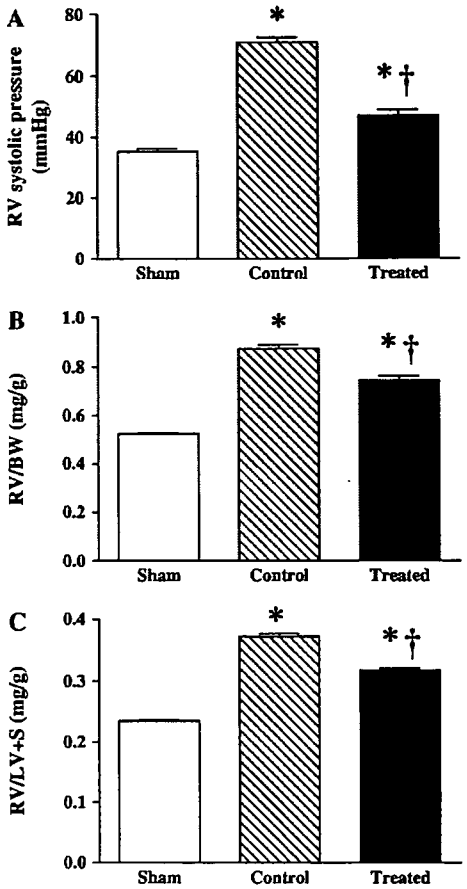

Figure 5. Effects of ONO-1301MS on pulmonary hemodynamics. (*A*) Effects of ONO-1301MS on right ventricular (RV) systolic pressure, (*B*) RV weight to body weight (RV/BW), and (C) RV weight to left ventricular plus septal weight (RV/LV + S). Sham = sham rats given vehicle; control = monocrotaline (MCT)-treated rats given vehicle; treated = MCT rats treated with ONO-1301MS. Data are mean ± SEM. $^{*}P < 0.05$ versus sham; $^{\dagger}P < 0.05$ versus control.

microspheres (ONO-1301MS) allowed a 3-week elevation of its circulating level, (2) ONO-1301MS had a sustained inhibitory effect on thromboxane synthase activity, and (3) a single subcutaneous administration of ONO-1301MS attenuated MCT-induced pulmonary hypertension in rats.

TABLE 1. PHYSIOLOGIC PROFILES OF THREE EXPERIMENTAL GROUPS

	Sham*	Control†	Treated‡
No. of rats	10	11	11
BW, g	203 ± 4	165 ± 7§	175 ± 3§
Heart rate, beats/min	454 ± 7	441 ± 10	445 ± 6
Mean arterial pressure, mm Hg	110 ± 2	111 ± 3	107 ± 2
LV + S/BW, mg/g	2.23 ± 0.02	2.34 ± 0.02§	2.34 ± 0.04§

Definition of abbreviations: BW = body weight; LV = left ventricle; LV + S/BW = LV plus septal weight to body weight ratio.

Data are mean ± SEM. These measurements were performed on Day 21.

* Sham = rats given vehicle.

† Control = MCT rats given vehicle.

‡ Treated = MCT rats treated with ONO-1301MS.

§ $P < 0.05$ versus sham.

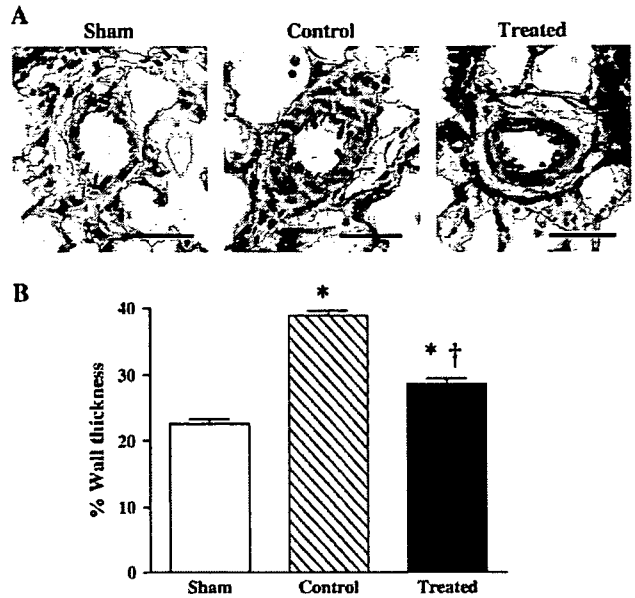

Figure 6. Effect of ONO-1301MS on vascular remodeling. (*A*) Representative photomicrographs of peripheral pulmonary arteries on Day 21. *Scale bars* = 50 μm. (*B*) Quantitative analysis of percentage of wall thickness in peripheral pulmonary arteries. Data are mean ± SEM. $^{*}P < 0.05$ versus sham; $^{\dagger}P < 0.05$ versus control.

Conventional prostacyclin and its analogs need continuous infusion or frequent administration because of their short duration of action. Previously, we reported a new type of prostacyclin agonist, ONO-1301, which has long-lasting prostacyclin activity and an inhibitory effect on thromboxane synthase (14). Although ONO-1301 has such interesting features, it still needs to be administered twice a day to achieve a significant improvement in pulmonary hypertension. To overcome this problem, we developed a new drug delivery system for prostacyclin. We polymerized ONO-1301 with PLGA microspheres to develop a novel sustained-release prostacyclin analog.

PLGA microspheres have been used as a controlled delivery system for bioactive agents (25). The release of bioactive agents from PLGA microspheres occurs through hydrolytic degradation of the polymeric matrix. Importantly, PLGA has already been used in humans. PLGA microspheres containing leuprorelin, a potent luteinizing hormone–releasing hormone analog, have been administered to patients with prostate and breast cancer by subcutaneous injection (26, 27). The rate of release of contents of PLGA microspheres can be changed by varying the factors affecting the hydrolytic degradation behavior of PLGA, such as lactate acid to glycolic acid ratio, average molecular weight of PLGA, and particle size (25). In the present study, we could control the degradation rate of ONO-1301MS. ONO-1301MS was designed to release ONO-1301 for 3 weeks, because it takes 3 weeks to induce pulmonary hypertension in rats after MCT injection. The present study demonstrated that the contained ONO-1301 was released for 3 weeks *in vitro*, producing a 3-week elevation of its circulating level after a single administration *in vivo*. It should be noted that only a single subcutaneous administration of ONO-1301MS attenuated MCT-induced pulmonary hypertension in rats. Thus, it might be possible to extend the administration interval for ONO-1301MS considerably longer than that with current prostacyclin analogs, and this could improve the quality of life in patients with pulmonary hypertension.

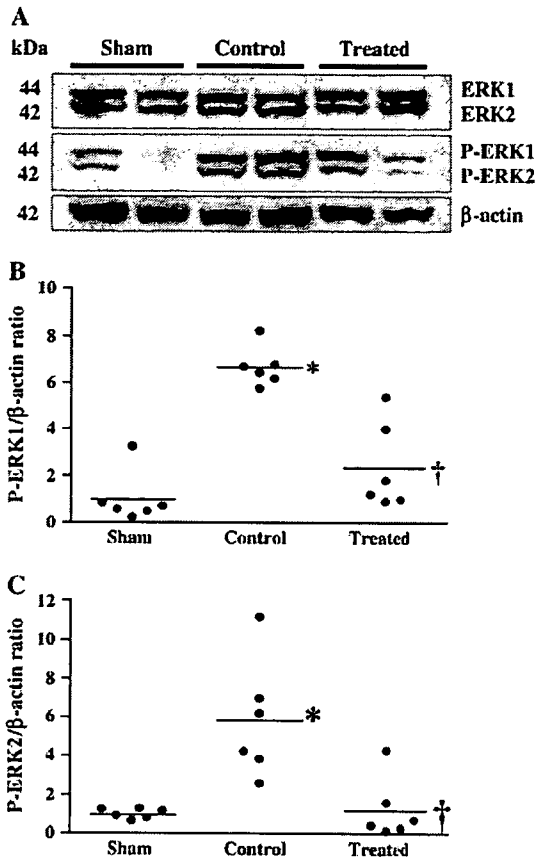

Figure 7. Effect of ONO-1301MS on extracellular signal-regulated protein kinase (ERK) phosphorylation. (*A*) Representative Western blotting for ERK, phospho-ERK (P-ERK) and β-actin (protein loading control) in lungs on Day 21 (n = 6 in each group). (*B* and *C*) Scatter plot of quantitative analysis of P-ERK expression in lung tissue. *Horizontal lines* in this figure show the mean value. $^*P < 0.05$ versus sham; $^\dagger P < 0.05$ versus control.

With regard to cAMP, which is a second messenger of prostacyclin and its analogs, it has been reported that plasma cAMP level remained increased after administration of prostacyclin analogs (23, 28). In our results, administration of ONO-1301MS increased the plasma cAMP level for over 2 weeks. This increase in plasma cAMP level was parallel to the change in plasma ONO-1301 level. In addition, ONO-1301MS attenuated the increase in urinary 11-DTXB$_2$ level in MCT rats 14 days after single administration. These results support that a single administration of ONO-1301MS produced a sustained beneficial effect for 3 weeks.

In the present study, we chose the maximum dose that did not induce significant hypotension. We did dose–response studies using ONO-1301MS (30, 100, and 300 mg/kg, respectively) (*see* Figure E1). ONO-1301MS at 300 mg/kg has induced significant hypotension. In addition, ONO-1301MS at 30 mg/kg did not significantly decrease RV systolic pressure (*see* Figure E3). On the other hand, ONO-1301MS at 100 mg/kg significantly decreased RV systolic pressure without significant hypotension. Furthermore, a single injection of 100 mg/kg ONO-1301 without PLGA or PLGA without ONO-1301 to MCT rats did not influence hemodynamics and vascular remodeling (*see* Figures E1–E3). These results suggest that a single injection of ONO-1301MS ameliorates MCT-induced pulmonary hypertension. Consistent with these hemodynamic data, RV/BW and medial wall thickness of pulmonary arteries, as indexes of RV hypertrophy and elevation of pulmonary arteriolar resistance, respectively, were significantly attenuated by the treatment with ONO-1301MS.

In histologic analysis, hypertrophy of pulmonary vessels after MCT injection was significantly attenuated by treatment with ONO-1301MS. An earlier clinical trial has shown that long-term therapy with epoprostenol significantly reduces pulmonary vascular resistance in patients who have no short-term response to vasodilators (5). It is speculated that such a beneficial effect of epoprostenol is caused not only by vasodilatation and antiplatelet aggregation but also by an antiproliferative effect on SMCs and reverse remodeling of pulmonary arteries. In the present study, phosphorylated ERK1/2 in the lung tissue was significantly increased after MCT injection. However, this increase was markedly attenuated by treatment with ONO-1301MS. ERK is the final component of the mitogen-activated protein kinase cascade. Prostacyclin has been shown to inhibit phosphorylation of ERK1/2 through the activation of cAMP (29). With respect to this signaling, protein kinase A (PKA), an intracellular effector of cAMP, has been shown to negatively regulate the Ras–ERK cascade by phosphorylating Raf and by preventing its association with active Ras (30). Furthermore, we previously reported that ONO-1301 inhibited pulmonary fibroblast proliferation through activation of the cAMP/PKA pathway (31). Therefore, it is interesting to speculate that ONO-1301MS may have antiproliferative effects on pulmonary vascular SMCs at least in part through inhibition of ERK via a cAMP-dependent pathway, although the precise mechanism remains to be elucidated.

ONO-1301MS significantly decreased urinary level of 11-DTXB$_2$, a metabolite of TXA$_2$. TXA$_2$ is a vasoconstrictor and a potent stimulator of platelet aggregation (32, 33). Moreover, it has been demonstrated that TXA$_2$ induces mitosis in vascular SMCs through activation of ERK (34, 35). It has been suggested that imbalance of thromboxane and prostacyclin plays an important role in the development of pulmonary hypertension (36). Previous reports showed that administration of thromboxane synthase inhibitor modestly attenuated pulmonary hypertension (37, 38). Thus, an inhibitory effect of ONO-1301MS on thromboxane synthase may also contribute to improvement in pulmonary hypertension.

In the present study, no adverse reactions, such as flushing, diarrhea, hypotension, renal dysfunction, or hepatic dysfunction, were observed in the treated group. However, further preclinical studies are necessary to confirm the safety and efficacy of ONO-1301MS before clinical trials start in patients with pulmonary arterial hypertension.

We did not measure cardiac output because of technical and mechanical problems. To support our hemodynamic data, we evaluated a variety of indexes, such as RV/BW and medial wall thickness of pulmonary arteries. These physiologic and histologic findings have been consistent with data on RV systolic pressure. Therefore, it is unlikely that the reduction in RV systolic pressure observed in the present study was related to the reduced cardiac output.

In conclusion, we developed a novel sustained-release prostacyclin analog polymerized with PLGA microspheres (ONO-1301MS), which achieved a 3-week elevation of its circulating level and simultaneously increased plasma cAMP levels for over 2 weeks, and had an inhibitory effect on thromboxane synthase. A single subcutaneous administration of ONO-1301MS attenuated MCT-induced pulmonary hypertension in rats. ONO-1301MS may have an antiproliferative effect through inhibition of ERK phosphorylation. This drug delivery system for a prostacyclin analog may be a new therapeutic strategy for the treatment of pulmonary arterial hypertension.

Conflict of Interest Statement: None of the authors has a financial relationship with a commercial entity that has an interest in the subject of this manuscript.

References

1. McLaughlin VV, McGoon MD. Pulmonary arterial hypertension. *Circulation* 2006;114:1417–1431.
2. Moncada S, Gryglewski R, Bunting S, Vane JR. An enzyme isolated from arteries transforms prostaglandin endoperoxides to an unstable substance that inhibits platelet aggregation. *Nature* 1976;263:663–665.
3. Moncada S, Vane JR. Arachidonic acid metabolites and the interactions between platelets and blood-vessel walls. *N Engl J Med* 1979;300: 1142–1147.
4. Humbert M, Sitbon O, Simonneau G. Treatment of pulmonary arterial hypertension. *N Engl J Med* 2004;351:1425–1436.
5. McLaughlin VV, Genthner DE, Panella MM, Rich S. Reduction in pulmonary vascular resistance with long-term epoprostenol (prostacyclin) therapy in primary pulmonary hypertension. *N Engl J Med* 1998;338:273–277.
6. McLaughlin VV, Shillington A, Rich S. Survival in primary pulmonary hypertension: the impact of epoprostenol therapy. *Circulation* 2002; 106:1477–1482.
7. Sitbon O, Humbert M, Nunes H, Parent F, Garcia G, Herve P, Rainisio M, Simonneau G. Long-term intravenous epoprostenol infusion in primary pulmonary hypertension: prognostic factors and survival. *J Am Coll Cardiol* 2002;40:780–788.
8. Okano Y, Yoshioka T, Shimouchi A, Satoh T, Kunieda T. Orally active prostacyclin analogue in primary pulmonary hypertension. *Lancet* 1997;349:1365.
9. Nagaya N, Uematsu M, Okano Y, Satoh T, Kyotani S, Sakamaki F, Nakanishi N, Miyatake K, Kunieda T. Effect of orally active prostacyclin analogue on survival of outpatients with primary pulmonary hypertension. *J Am Coll Cardiol* 1999;34:1188–1192.
10. Olschewski H, Simonneau G, Galie N, Higenbottam T, Naeije R, Rubin LJ, Nikkho S, Speich R, Hoeper MM, Behr J, *et al.* Inhaled iloprost for severe pulmonary hypertension. *N Engl J Med* 2002;347:322–329.
11. Simonneau G, Barst RJ, Galie N, Naeije R, Rich S, Bourge RC, Keogh A, Oudiz R, Frost A, Blackburn SD, *et al.* Continuous subcutaneous infusion of treprostinil, a prostacyclin analogue, in patients with pulmonary arterial hypertension: a double-blind, randomized, placebo-controlled trial. *Am J Respir Crit Care Med* 2002;165:800–804.
12. Badesch DB, McLaughlin VV, Delcroix M, Vizza CD, Olschewski H, Sitbon O, Barst RJ. Prostanoid therapy for pulmonary arterial hypertension. *J Am Coll Cardiol* 2004;43:56S–61S.
13. Laliberte K, Arneson C, Jeffs R, Hunt T, Wade M. Pharmacokinetics and steady-state bioequivalence of treprostinil sodium (Remodulin) administered by the intravenous and subcutaneous route to normal volunteers. *J Cardiovasc Pharmacol* 2004;44:209–214.
14. Kataoka M, Nagaya N, Satoh T, Itoh T, Murakami S, Iwase T, Miyahara Y, Kyotani S, Sakai Y, Kangawa K, *et al.* A long-acting prostacyclin agonist with thromboxane inhibitory activity for pulmonary hypertension. *Am J Respir Crit Care Med* 2005;172:1575–1580.
15. Alonso MJ, Gupta RK, Min C, Siber GR, Langer R. Biodegradable microspheres as controlled-release tetanus toxoid delivery systems. *Vaccine* 1994;12:299–306.
16. Seagal J, Edry E, Keren Z, Leider N, Benny O, Machluf M, Melamed D. A fail-safe mechanism for negative selection of isotype-switched B cell precursors is regulated by the Fas/FasL pathway. *J Exp Med* 2003;198:1609–1619.
17. Mullerad J, Cohen S, Benharroch D, Apte RN. Local delivery of IL-1 alpha polymeric microspheres for the immunotherapy of an experimental fibrosarcoma. *Cancer Invest* 2003;21:720–728.
18. Mullerad J, Cohen S, Voronov E, Apte RN. Macrophage activation for the production of immunostimulatory cytokines by delivering interleukin 1 via biodegradable microspheres. *Cytokine* 2000;12:1683–1690.
19. Sanchez A, Gupta RK, Alonso MJ, Siber GR, Langer R. Pulsed controlled-released system for potential use in vaccine delivery. *J Pharm Sci* 1996;85:547–552.
20. Roullin VG, Lemaire L, Venier-Julienne MC, Faisant N, Franconi F, Benoit JP. Release kinetics of 5-fluorouracil-loaded microspheres on an experimental rat glioma. *Anticancer Res* 2003;23:21–25.
21. Kimura H, Kasahara Y, Kurosu K, Sugito K, Takiguchi Y, Terai M, Mikata A, Natsume M, Mukaida N, Matsushima K, *et al.* Alleviation of monocrotaline-induced pulmonary hypertension by antibodies to monocyte chemotactic and activating factor/monocyte chemoattractant protein-1. *Lab Invest* 1998;78:571–581.
22. Ono S, Voelkel NF. PAF antagonists inhibit monocrotaline-induced lung injury and pulmonary hypertension. *J Appl Physiol* 1991;71:2483–2492.
23. Itoh T, Nagaya N, Fujii T, Iwase T, Nakanishi N, Hamada K, Kangawa K, Kimura H. A combination of oral sildenafil and beraprost ameliorates pulmonary hypertension in rats. *Am J Respir Crit Care Med* 2004;169:34–38.
24. Fiorucci S, Mencarelli A, Meneguzzi A, Lechi A, Morelli A, del Soldato P, Minuz P. NCX-4016 (NO-aspirin) inhibits lipopolysaccharide-induced tissue factor expression in vivo: role of nitric oxide. *Circulation* 2002;106:3120–3125.
25. Shive MS, Anderson JM. Biodegradation and biocompatibility of PLA and PLGA microspheres. *Adv Drug Deliv Rev* 1997;28:5–24.
26. Fornara P, Jocham D. Clinical study results of the new formulation leuprorelin acetate three-month depot for the treatment of advanced prostate carcinoma. *Urol Int* 1996;56:18–22.
27. Schmid P, Untch M, Kosse V, Bondar G, Vassiljev L, Tarutinov V, Lehmann U, Maubach L, Meurer J, Wallwiener D, *et al.* Leuprorelin acetate every-3-months depot versus cyclophosphamide, methotrexate, and fluorouracil as adjuvant treatment in premenopausal patients with node-positive breast cancer: the TABLE study. *J Clin Oncol* 2007;25:2509–2515.
28. Beghetti M, Reber G, de Moerloose P, Vadas L, Chiappe A, Spahr-Schopfer I, Rimensberger PC. Aerosolized iloprost induces a mild but sustained inhibition of platelet aggregation. *Eur Respir J* 2002; 19:518–524.
29. Li RC, Cindrova-Davies T, Skepper JN, Sellers LA. Prostacyclin induces apoptosis of vascular smooth muscle cells by a cAMP-mediated inhibition of extracellular signal-regulated kinase activity and can counteract the mitogenic activity of endothelin-1 or basic fibroblast growth factor. *Circ Res* 2004;94:759–767.
30. Cook SJ, McCormick F. Inhibition by cAMP of Ras-dependent activation of Raf. *Science* 1993;262:1069–1072.
31. Murakami S, Nagaya N, Itoh T, Kataoka M, Iwase T, Horio T, Miyahara Y, Sakai Y, Kangawa K, Kimura H. Prostacyclin agonist with thromboxane synthase inhibitory activity (ONO-1301) attenuates bleomycin-induced pulmonary fibrosis in mice. *Am J Physiol Lung Cell Mol Physiol* 2006;290:L59–L65.
32. Hamberg M, Svensson J, Samuelsson B. Prostaglandin endoperoxides: a new concept concerning the mode of action and release of prostaglandins. *Proc Natl Acad Sci USA* 1974;71:3824–3828.
33. Svenssen J, Strandberg K, Tuvemo T, Hamberg M. Thromboxane A2: effects on airway and vascular smooth muscle. *Prostaglandins* 1977; 14:425–436.
34. Sachinidis A, Flesch M, Ko Y, Schror K, Bohm M, Dusing R, Vetter H. Thromboxane A2 and vascular smooth muscle cell proliferation. *Hypertension* 1995;26:771–780.
35. Morinelli TA, Tempel GE, Jaffa AA, Silva RH, Naka M, Folger W, Halushka PV. Thromboxane A2/prostaglandin H2 receptors in streptozotocin-induced diabetes: effects of insulin therapy in the rat. *Prostaglandins* 1993;45:427–438.
36. Christman BW, McPherson CD, Newman JH, King GA, Bernard GR, Groves BM, Loyd JE. An imbalance between the excretion of thromboxane and prostacyclin metabolites in pulmonary hypertension. *N Engl J Med* 1992;327:70–75.
37. Nagata T, Uehara Y, Hara K, Igarashi K, Hazama H, Hisada T, Kimura K, Goto A, Omata M. Thromboxane inhibition and monocrotaline-induced pulmonary hypertension in rats. *Respirology* 1997;2:283–289.
38. Rich S, Hart K, Kieras K, Brundage BH. Thromboxane synthetase inhibition in primary pulmonary hypertension. *Chest* 1987;91:356–360.

J Appl Physiol 104: 88–96, 2008.
First published October 25, 2007; doi:10.1152/japplphysiol.00610.2007.

Changes in macrovessel pulmonary blood flow distribution following chronic hypoxia: assessed using synchrotron radiation microangiography

Daryl O. Schwenke,[1,2] James T. Pearson,[3] Kenji Kangawa,[1] Keiji Umetani,[4] and Mikiyasu Shirai[5]

[1]Department of Biochemistry, National Cardiovascular Center Research Institute, Suita, Osaka, Japan; [2]Department of Physiology, University of Otago, Dunedin, New Zealand; [3]Department of Physiology and Monash Centre for Synchrotron Science, Monash University, Melbourne, Australia; [4]Japan Synchrotron Radiation Research Institute, Hyogo, Japan; and [5]Faculty of Health Sciences, Hiroshima International University, Hiroshima, Japan

Submitted 10 June 2007; accepted in final form 22 October 2007

Schwenke DO, Pearson JT, Kangawa K, Umetani K, Shirai M. Changes in macrovessel pulmonary blood flow distribution following chronic hypoxia: assessed using synchrotron radiation microangiography. *J Appl Physiol* 104: 88–96, 2008. First published October 25, 2007; doi:10.1152/japplphysiol.00610.2007.—Structural and functional changes of the pulmonary circulation, particularly during the pathogenesis of pulmonary arterial hypertension (PAH), remain to be fully elucidated. In this study, we utilized monochromatic synchrotron radiation (SR) microangiography to assess changes in pulmonary arteriole blood flow in the intact-chest rat after 4 wk of chronic hypoxia. Sprague-Dawley rats were exposed to normoxia (N-rats) or chronic hypoxia (10% O_2; CH-rats) for 28 days. Rats were anesthetized, and microangiography was performed on the left lung to assess *1*) the branching distribution of pulmonary arteriole blood flow (internal diameter >80 μm) and *2*) dynamic changes in vessel lumen diameter during acute hypoxic (8% O_2 for 4 min) pulmonary vasoconstriction (HPV) before and after β-adrenoceptor blockade (2 mg/kg iv propranolol). Using SR angiography, we observed that the number of opaque third- and fourth-generation vessels (100–300 μm) for CH-rats was significantly fewer than the number for N-rats. The magnitude of HPV was not different between CH-rats and N-rats. β-Adrenoceptor blockade accentuated the HPV in 200- to 300-μm vessels for CH-rats, but even more so in N-rats. However, in CH-rats, β-adrenoceptor blockade also accentuated the HPV in 100- to 200-μm vessels. In summary, we utilized SR to assess gross blood flow changes and functional changes (i.e., HPV) of the pulmonary circulation in PAH. These results highlight the benefits of SR for assessing pulmonary circulatory pathology. Of particular importance, future use of SR will provide an effective method for assessing potential therapeutic treatments for PAH.

pulmonary microvessels; hypoxia; intact chest; rat

ALVEOLAR HYPOXIA, A POTENTIAL adverse complication associated with numerous respiratory disorders, causes pulmonary vasoconstriction, which is reversible on reoxygenation. However, when sustained, the elevated shear stress within the pulmonary vasculature causes endothelial cell injury dysfunction (2), ultimately leading to the pathogenesis of pulmonary arterial hypertension (PAH). PAH is characterized by irreversible vascular remodeling and medial thickening of thin muscular-walled vessels (100–300 μm), as well as the formation of new muscle around nonmuscular or partially muscular vessels (50–150 μm) (12, 23, 24, 31). The ensuing decrease in vessel internal caliber increases pulmonary vascular resistance and, consequently, increases the workload of the heart, enhances the risk of heart failure, and is, therefore, closely associated with an increased mortality.

Several studies have indicated that the increase in pulmonary vascular resistance is further exacerbated during chronic hypoxia by a reduction in the number of perfused blood vessels within the pulmonary vascular bed, due to either vessel occlusion (i.e., extensive medial thickening) or the loss of vessels, also known as "rarefaction" or "pruning" of small vessels (8, 11, 25). More recent evidence, however, has cast doubt on this paradigm, with some reports now indicating that angiogenesis is evident within the pulmonary circulation during chronic hypoxia (13, 14, 16).

The underlying mechanisms governing the pathogenesis of PAH remain to be fully elucidated. One of the limitations in understanding the pathology of the lung has been the inability to clearly visualize blood flow within the pulmonary vascular bed. More conventional methods of assessing the vascular anatomy of the diseased lung necessitate removal of the lung from the animal (i.e., in vitro) for angiography (i.e., X-ray) or microsection analysis. Conventional angiography methods have considerable limitations in visualizing the vessels that are most susceptible to pathological changes, i.e., <200 μm (37, 40). Therefore, a technique for visualizing the pulmonary circulation within a closed-chest model, i.e., under intact neurohumoral regulation, is required to better understand the structural and functional changes in vivo and, ultimately, to assess specific treatments for lung disorders more reliably.

In a recent study, we (32) demonstrated the validity and accuracy of synchrotron radiation (SR) microangiography for visualizing pulmonary blood flow within vessels in a closed-chest rat model and for assessing dynamic changes in vessel caliber associated with acute hypoxic pulmonary vasoconstriction (HPV). Although resolution limitations of SR only enabled vessels with an internal diameter >80 μm to be visualized, many vessels that are susceptible to pathological changes during chronic hypoxia are well within the resolution capabilities of SR. In contrast to conventional angiography systems, SR is characterized by high brilliance and extreme collimation (36), allowing enhanced sensitivity to contrast material and superior image quality in terms of spatial and density resolution because divergence and scatter of X-ray photons are eliminated.

The primary aim of this study was to utilize SR microangiography to effectively highlight changes in pulmonary blood flow

Address for reprint requests and other correspondence: D. O. Schwenke, Dept. of Physiology, Univ. of Otago, PO Box 56, Dunedin, New Zealand (e-mail: daryl.schwenke@stonebow.otago.ac.nz).

The costs of publication of this article were defrayed in part by the payment of page charges. The article must therefore be hereby marked "*advertisement*" in accordance with 18 U.S.C. Section 1734 solely to indicate this fact.

distribution, following the pathogenesis of chronic hypoxia-induced PAH. Because of the resolution limitations of SR, we only assessed those pulmonary arterioles with an internal diameter >80 μm. The structural changes in the pulmonary circulation associated with chronic hypoxia have been shown to alter the functional properties of the pulmonary vasculature, in particular, the vasoconstriction response to acute hypoxia (i.e., HPV) (19, 22). This altered HPV has been attributed, at least in part, to the modulatory effects of the sympathetic nervous system on the pulmonary vasculature (33, 35). Therefore, we also aimed to utilize the high definition of SR to assess the adverse changes in pulmonary reactivity to acute hypoxia and, furthermore, to distinguish the local intrinsic response (i.e., HPV) from that of the extrinsic neural response (i.e., sympathetic modulation) by using propranolol to inhibit β-adrenoceptor activation.

MATERIALS AND METHODS

Animals. Experiments were conducted on 10 male Sprague-Dawley rats (10 wk old; ~220–320 g body wt). All rats were on a 12:12-h light-dark cycle at 25 ± 1°C and were provided with food and water ad libitum. Rats were housed in standard normoxic conditions (n = 5) or were continuously housed in a hypoxic chamber (10 ± 0.1% O_2) for 4 wk (n = 5), except for a 10-min interval each day when the chamber was cleaned. The hypoxic gas mixture was prepared from N_2 (gas cylinders) and compressed air and was continuously delivered to the hypoxic chamber (30 liter capacity) at a flow rate of ~8 l/min. All experiments were approved by the local Animal Ethics Committee and conducted in accordance with the guidelines of the Physiological Society of Japan.

Anesthesia and surgical preparation. Rats were anesthetized with pentobarbital sodium (60 mg/kg ip). Supplementary doses of anesthetic were periodically administered (~15 $mg \cdot kg^{-1} \cdot h^{-1}$ ip). Throughout the experimental protocol, body temperature was maintained at 37°C using a rectal thermistor coupled with a thermostatically controlled heating pad.

The trachea was cannulated, and the lungs were ventilated with a rodent ventilator (SN-480-7; Shinano, Tokyo, Japan). The inspirate gas was enriched with O_2 (~50% O_2), and the ventilator settings were adjusted (tidal volume ~3.5 ml; frequency of ~70 /min). A femoral artery and vein were cannulated for measurement of systemic arterial blood pressure (ABP) and drug administration, respectively. A 20-gauge BD Angiocath catheter (Becton Dickinson), with the tip at a 30-degree angle, was inserted into the jugular vein and advanced into the right ventricle for administering contrast agent and intermittently measuring right ventricular pressure (RVP).

The rat was securely fastened to a clear Perspex surgical plate, which had a single window opening directly beneath the thorax area. The surgical plate was then fixed in a vertical position in front of the beam pathway, so that the synchrotron beam could pass perpendicular to the sagittal plane from anterior to posterior through the rat thorax and ultimately to a SATICON X-ray camera described below.

Microangiographic system. The pulmonary circulation was visualized with SR microangiography at the SPring-8 BL28B2 beam-line facility (Hyogo, Japan). The use of SR for visualizing the pulmonary microcirculation in the closed-chest rat has previously been described in detail (32).

In brief, SR has a broad and continuous spectrum from the infrared to the X-ray regions. A single crystal monochromator was used to select a single energy of SR, producing X-rays of a very narrow energy bandwidth for imaging. This SR system comprised a monochromatic 33.2-keV X-ray source, just above the iodine K-edge energy for maximal contrast.

X-rays transmitted through the rats were detected by an X-ray detector (Hitachi Denshi Techno-System, Tokyo, Japan) incorporating a SATICON X-ray pickup tube (Hamamatsu Photonics, Shizuoka, Japan). The biomedical imaging SATICON X-ray camera has a resolution of 1,050 scanning lines and can record images at a maximum speed of 30 frames/s for up to 30 s. The shutter open time used in this study was 2.6–3.0 ms/frame. The detector features a 9.5-μm equivalent pixel size projected onto the input area and an input field size of 9.5 × 9.5 mm. High-resolution images were stored in a digital frame memory system with 1,024 × 1,024 pixel format and 10-bit resolution.

Experimental protocol. The rat was positioned in front of the beam line so that the upper segment of the left lobe was positioned in front of the SATICON X-ray camera in alignment with the 9.5 × 9.5-mm imaging field (i.e., between the 2nd and 3rd rib; Fig. 1). Subsequently, baseline heart rate (HR), RVP, and ABP data were collected. Immediately before vessels were imaged, the three-way stopcock on the right ventricle catheter was opened to a clinical autoinjector (Nemoto Kyorindo, Tokyo, Japan), which was used to inject a single bolus of contrast agent (Iomeron 350; Eisai, Tokyo, Japan) at high speed (0.4 ml/s). For each 2-s period of scanning, 100 frames were recorded. Rats were given at least 10 min to recover from each injection of contrast agent. Regular inspection between contrast injections confirmed that the pulmonary vasculature was clear of agent within this period of time.

After baseline imaging was completed, rats were exposed to acute hypoxia (8% O_2 in N_2) for 4 min. During acute hypoxia, ABP, HR, and RVP data were continuously recorded until the 3rd min, after which recording of RVP was stopped, and the catheter was switched from the pressure transducer to the clinical injector for imaging. Lung microangiography was performed on the hypoxic lung after the 4th min of hypoxia.

After recovery from the acute hypoxic test, rats were administered the β-receptor blocker propranolol (2 mg/kg iv). After 10–15 min was allowed for all cardiovascular variables to stabilize, pulmonary microangiography was repeated before and after acute hypoxia.

Data acquisition and analysis. The RVP and ABP signals were detected by separate Deltran pressure transducers (Utah Medical Products), and the signals were relayed to PowerLab bridge amplifiers (ML117, ADInstruments) and then continuously sampled at 500 Hz with an eight-channel MacLab/8s interface hardware system (ADInstruments) and recorded on a Macintosh Power Book G4 using Chart software (version 5.0.1, ADInstruments). HR was derived from the arterial systolic peaks.

From the 2-s period of image collection, one frame per scan (one scan = 100 frames) was selected for image enhancement and analysis. Furthermore, only those frames recorded at, or near, end systole were used for assessing and comparing pulmonary vessel diameter between baseline and hypoxic conditions.

All imaged vessel branches were counted. Where possible, the widths of two to four vessels of each branching generation (2nd to 4th

Fig. 1. A schematic drawing of the arterial circulation of the left lung in a rat. The square box represents the position of the 9.5 × 9.5-mm imaging window used for microangiography of the pulmonary microvessels. [Reprinted from Schwenke et al. (32).]

generation) were measured to ensure that a wide variety of vessel sizes was selected from each frame. Vessels were categorized according to internal diameter: 100–200, 200–300, 300–500, and >500 μm. The internal diameter of individual vessels was measured before and after acute hypoxia, with and without β-receptor blockade (i.e., propranolol treatment).

Image analysis. The computer-imaging program Image Pro-plus (version 4.1, Media Cybernetics) was used to enhance the contrast and clarity of angiogram images. To enhance images, a temporal subtraction operation was performed for flat-field correction using summation results of 10 consecutive frames acquired before contrast agent injection. The summation image taken before injection was subtracted from a single raw image taken after injection to eliminate the superimposed background structure.

Image Pro-plus was also used to evaluate the vessel internal diameter. A 100-μm-thick tungsten filament, which had been placed directly across the corner of the detector's window, appeared in all of the recorded images and was subsequently used as a reference for calculating vessel diameter (μm). The line-profile function of Image Pro-plus was used to measure changes in pixel intensity (brightness) along manually drawn segments spanning 10–40 pixels on either side in the direction perpendicular to the vessel (see Fig. 2). The first edge of the vessel was determined as the pixel at which intensity decreased by 1.5 standard deviations below that of the preceding 10–40 pixels (depending on space between vessels). The opposite criterion was applied to ascertain the distal edge of the vessel. This boundary segmentation procedure was performed at two different points along the length of the vessel, and the average of the two values was used for data collation. To assess reproducibility, the procedure for measuring vessel width was repeated by a second observer. Of the total number of vessels analyzed (91 vessels from normoxic and chronic hypoxic rats; see RESULTS), 50 vessels from various branching generations were randomly selected from the appropriate angiograph image for analyses by a second observer. The value for each vessel width that was analyzed by both observers was highly reproducible. Regression analysis indicated that the measurements from both observers were highly correlated ($y = 6.752 + 0.983x$, $r^2 = 0.975$) and had an average difference of 6 ± 3 μm (for 100- to 200-μm vessels) to 9 ± 4 μm (for 300–500 μm).

Evaluation of accuracy of measurement. We (32) have previously described in detail the method of evaluating the accuracy of measurement. In brief, we estimated a margin of error for detecting the edge of a vessel by assessing pixel variability of the reference wire (known diameter of 100 μm). Before commencing the study, we measured wire width at 40 random points along its length. The mean width of this reference wire was 12.99 pixels (SD ± 1.12). This equates to an average pixel size of 7.69 μm (95% confidence interval of 7.496–7.908 μm). Consequently, the 100-μm tungsten wire could accurately be measured to within ~5 μm (range of 97.4–102.7 μm).

In this study, the iodine contrast agent was injected into the right ventricle so that the iodine concentration within the pulmonary circulation would have been diluted, which is likely to have attenuated X-ray absorption and potentially the accuracy of the vessel width measurement. We previously performed preliminary phantom measurements to assess the relationship between X-ray absorption and iodine concentration. The phantom measurements consisted of filling nine tubes, with an internal diameter of 200 μm, with various concentrations of iodinated contrast material ranging from pure agent (370 mg/cm³) to distilled water (i.e., 0 mg/cm³). The line-profile function of Image Pro-plus was used to assess the magnitude of absorption (i.e., brightness) for each concentration of iodinated contrast material (Fig. 2).

The widths of tubes containing an iodine concentration between 32 and 370 mg/cm³ could be accurately measured with a small margin of error, e.g., the width of the tube containing 32 mg/cm³ iodine was measured at 40 points and had a 95% confidence interval of 196.84–203.26 μm. This is a margin of error similar to that obtained for multiple measurements of the tungsten reference wire.

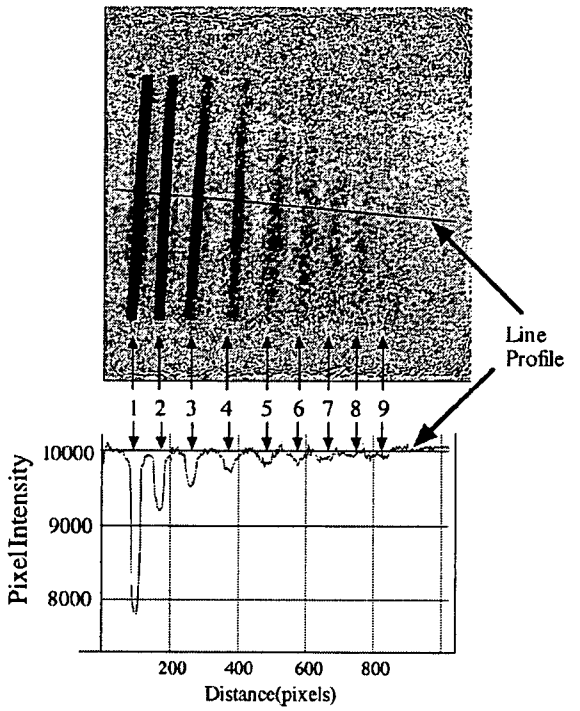

Fig. 2. *Top*: an angiograph image obtained from a phantom study that assessed X-ray absorption of 9 tubes containing *1*) Iopamiron 370 (370 mg/cm³ iodine; Nihon Schering), *2*) 127 mg/cm³ iodine (diluted contrast material with distilled water), *3*) 64 mg/cm³ iodine, *4*) 32 mg/cm³ iodine, *5*) 12.8 mg/cm³ iodine, *6*) 6.4 mg/cm³ iodine, *7*) 1.28 mg/cm³ iodine, *8*) distilled water, and *9*) air. A 5-mm-thick aluminum mask was overlaid to simulate attenuation by the animal body. Concentrations ranging from 32 to 127 mg/cm³ of iodine simulate typical in vivo conditions for intra-arterial injection techniques. *Bottom*: computerized line profile (representing the solid line transecting all 9 tubes in *top*) was performed to show that changes in pixel intensity (i.e., brightness), which reflect the magnitude of absorption, are dependent on iodine concentration.

These results show that measurements of 200 μm in diameter can be made precisely for those vessels with an iodine concentration of >32 mg/cm³. Moreover, it seems reasonable to suppose that measurements of ~100 μm in diameter can be made with the required precision for those vessels with an iodine concentration of 64 mg/cm³ or greater.

Statistical analysis. All statistical analyses were conducted with Statview (version 5.01; SAS Institute). All results are presented as means ± SE. Two-way ANOVA (repeated measures) was used to test whether propranolol significantly altered the dynamic pulmonary vasoconstriction response to acute hypoxia. One-way ANOVA (factorial) was used to test for differences in *1*) vessel caliber during normoxia and acute hypoxia and *2*) baseline values for normoxic rats (N-rats) compared with chronic hypoxic rats (CH-rats). Where statistical significance was reached, post hoc analyses were incorporated using the paired or unpaired *t*-test with the Dunnett's correction for multiple comparisons. A P value ≤0.05 was predetermined as the level of significance for all statistical analysis.

RESULTS

Baseline. Rats had an initial body weight of ~285 g before being placed into a normoxic (N-rats) or hypoxic chamber (CH-rats) for 4 wk. The gain in body weight of CH-rats (~20%

increase) was significantly lower ($P < 0.01$) than that for N-rats (~74% increase) over the 4-wk period. Chronic hypoxia induced PAH (see Table 1), as demonstrated by our observation that systolic RVP of CH-rats was ~120% higher than that of N-rats ($P < 0.01$). Chronic hypoxia did not significantly alter mean ABP (MABP) or HR.

Using SR, we were able to clearly visualize the blood flow of pulmonary microvessels (>80 μm) in the left lung of both N-rats and CH-rats. The typical branching pattern of the pulmonary circulation from the main axial artery of the left lobe to the fourth generation of branching (within the 9.5 × 9.5 mm imaging window) of a N-rat and a CH-rat is presented below (see Fig. 4).

The internal diameter of 52 vessels was measured in five N-rats: 24 vessels with a diameter between 100 and 200 μm, 15 vessels with a diameter between 200 and 300 μm, 7 vessels with a diameter between 300 and 500 μm, and 6 vessels with a diameter >500 μm. In comparison, CH-rats had comparatively fewer vessels (Fig. 3*A*); thus the internal diameter of 39 vessels was measured in five CH-rats: 15 vessels with a diameter between 100 and 200 μm, 10 vessels with a diameter between 200 and 300 μm, 7 vessels with a diameter between 300 and 500 μm, and 7 vessels with a diameter >500 μm.

The total number of vessel branches visible within each baseline image (i.e., 9.5 × 9.5-mm imaging window) was counted. As illustrated in Fig. 3*A*, the number of opaque third- and fourth-generation vessels for CH-rats (9 ± 1 and 16 ± 2 vessels, respectively) was significantly fewer than the number for N-rats (14 ± 1 and 30 ± 2 vessels, respectively; $P < 0.05$). The numbers of first- and second-generation branches were not significantly different between N-rats and CH-rats (2 and 4 or 5, respectively).

Vessel caliber tended to decrease according to each generation of branching, as well as the distance away from the main axial artery toward the periphery (Fig. 3*B*). However, often more than one size category could be found within one branching generation. For example, the third generation of branching (135–290 μm) comprised vessels of the 100- to 200-μm and 200- to 300-μm categories (Fig. 3*B*). The internal diameter of the first-generation branch in CH-rats (740 ± 53 μm) was significantly larger than that shown in N-rats (511 ± 57 μm; $P < 0.05$), possibly because of the higher distending pressure (i.e., pulmonary arterial pressure) for CH-rats. Vessel caliber was not significantly different between N-rats and CH-rats for the second generation (210–570 μm), third generation (135–290 μm), and fourth generation of branching (90–180 μm) (Fig. 3*B*).

Table 1. *Systolic RVP, MABP, and HR data of anesthetized N-rats and CH-rats before and after propranolol administration*

	Systolic RVP, mmHg	MABP, mmHg	HR, beats/min
	Saline		
N-rats	24.3±1.0	103±7	338±13
CH-rats	53.1±2.0†	118±4	353±13
	Propranolol (2 mg/kg iv)		
N-rats	27.3±1.4	105±6	319±4
CH-rats	54.2±1.7†	136±3*†	294±5*†

Values are means ± SE. N-rats, normoxic rats ($n = 5$); CH-rats, chronic hypoxic rats ($n = 5$); RVP, right ventricular pressure; MABP, mean arterial blood pressure; HR, heart rate. *Significant difference between saline and propranolol ($P < 0.01$). †Significant difference between N-rats and CH-rats ($P < 0.01$).

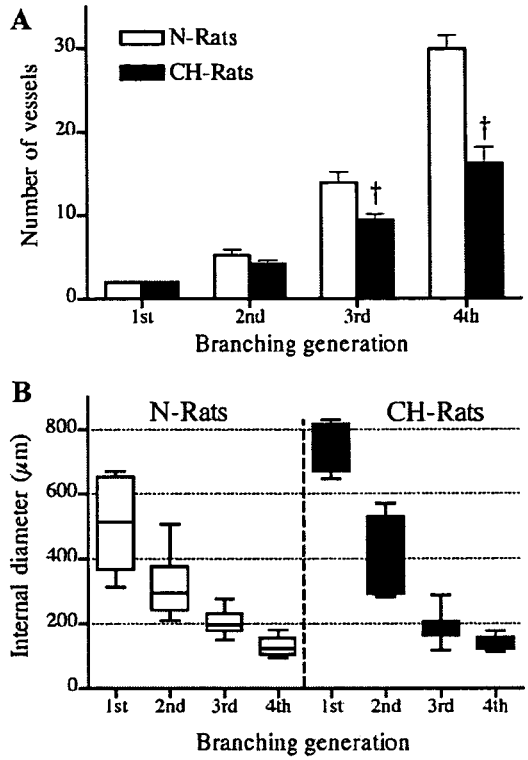

Fig. 3. Changes in the number of opaque vessels (means ± SE) (*A*) and range of vessel sizes (box and whisker graph; *B*) at each of the first 4 branching generations of the pulmonary circulation in normoxic rats (N-rats; $n = 5$) and chronic hypoxic rats (CH-rats; $n = 5$). †Significant difference between N-rats and CH-rats ($P < 0.05$).

Responses to acute hypoxia. N-rats and CH-rats were exposed to 8% O_2 for 4 min. Acute hypoxia caused a significant decrease in the internal diameter of all vessels with an internal diameter <500 μm (for N-rats) or <300 μm (for CH-rats) (Figs. 4 and 5). In both groups of rats, the magnitude of constriction tended to increase as vessel caliber decreased, with the greatest degree of vasoconstriction occurring in those vessels with a diameter between 100 and 300 μm. These vessels were generally of the third to fourth generation of branching. There was no significant difference between N-rats and CH-rats regarding the magnitude of HPV for all vessel sizes.

The magnitudes of responses to hypoxia for systolic RVP, MABP, and HR are presented in Fig. 6. Acute hypoxia induced a significant 21% increase in systolic RVP ($P < 0.01$) in N-rats, which was not significantly different from that observed in CH-rats (27% increase above baseline). This increase in systolic RVP reflects the HPV seen with microangiography. Hypoxia decreased MABP in CH-rats, but significantly more so in N-rats (40% and 54% decrease, respectively). Hypoxia did not alter HR in either N-rats or CH-rats.

Responses to propranolol. N-rats and CH-rats were administered the β-receptor blocker propranolol (2 mg/kg iv). Propranolol did not significantly alter baseline pulmonary vessel

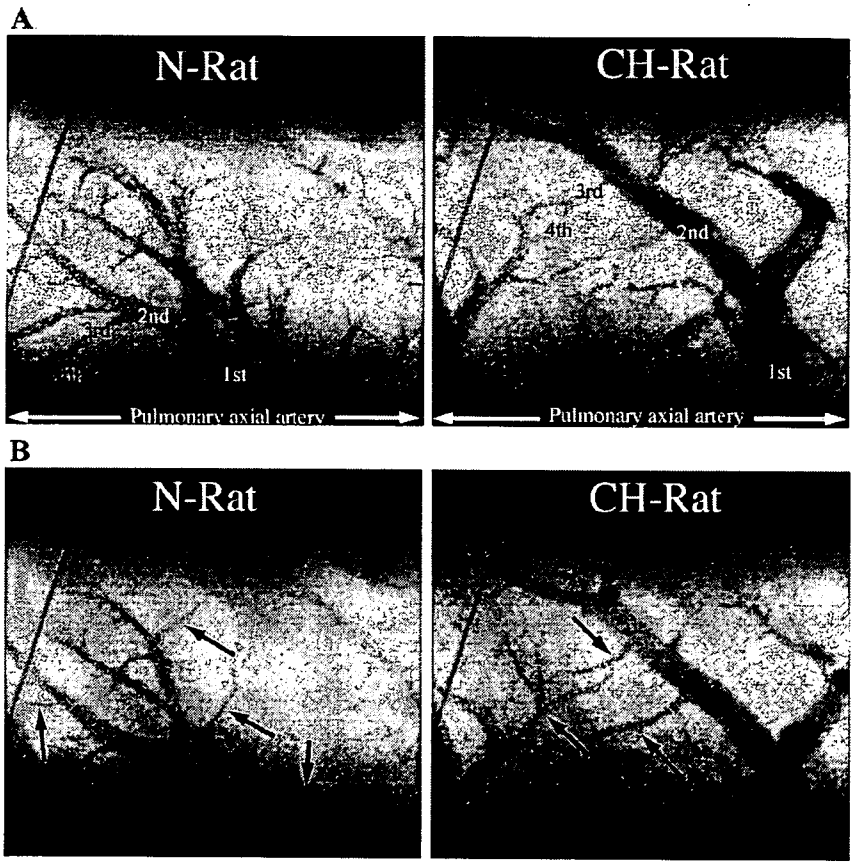

Fig. 4. Typical microangiogram images showing the branching pattern of small pulmonary arteries in N-rats (n = 5) and CH-rats (n = 5). Pulmonary branches to the 4th generation from the left main axial artery (not in the image) were visible. The tungsten wire in the *top left* of each image is a reference of 100 μm diameter. Images were recorded during air breathing (*A*) and after 4 min of acute hypoxia (8% O_2; *B*). Images for *A* and *B* were obtained from the same respective N-rat or CH-rat. The black arrows point to branches of the pulmonary vessels that have constricted in response to hypoxia.

caliber for any of the vessel size groups analyzed, in both N-rats and CH-rats. The lack of effect of propranolol on pulmonary vessel caliber for N-rats and CH-rats was reflected in the insignificant response of systolic RVP to propranolol (Table 1). In N-rats, propranolol did not significantly alter MABP or HR. In CH-rats, propranolol significantly increased MABP (15% increase) and caused a 17% decrease in HR ($P < 0.01$).

In N-rats, β-receptor blockade significantly exacerbated the magnitude of acute hypoxic vasoconstriction in 200- to 300-μm-sized pulmonary vessels (Fig. 5). However, the systolic RVP, MABP, and HR responses to acute hypoxia were unaltered (Fig. 6). In comparison, β-receptor blockade in CH-rats significantly accentuated the systolic RVP response to acute hypoxia ($P < 0.05$), reflecting extensive pulmonary vasoconstriction in 200- to 300-μm-sized vessels and, unlike that observed for N-rats, even greater constriction in 100- to 200-μm-sized vessels (Fig. 5). The HPV response of vessels with a caliber >300 μm was not altered by β-receptor blockade in N-rats or CH-rats.

DISCUSSION

This study has demonstrated the effectiveness of SR for visualizing the adverse anatomic and functional changes of the pulmonary circulation associated with the pathogenesis of pulmonary hypertension in a closed-chest rat model.

PAH. Although significant advances in the treatment of pulmonary disorders have been made in recent decades, the

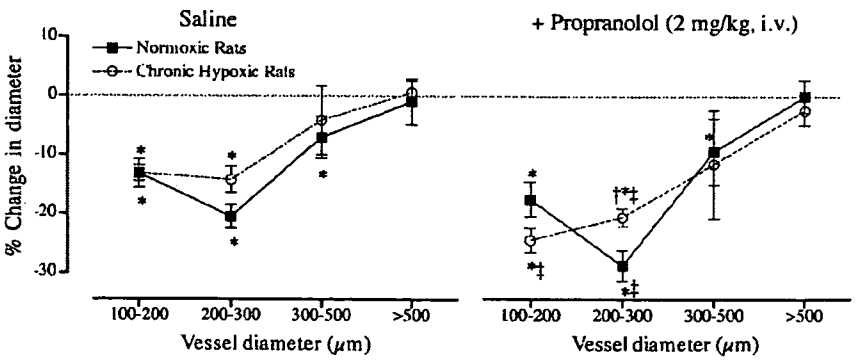

Fig. 5. Relationship between vessel size and the magnitude of pulmonary vasoconstriction (%decrease in vessel diameter) in response to acute hypoxia (8% O_2 for 4 min) in N-rats (n = 5) and CH-rats (n = 5) before (*left*) and after (*right*) intravenous administration of propranolol (2 mg/kg). *Significant vasoconstriction response to acute hypoxia ($P < 0.05$). †Significant difference between N-rats and CH-rats ($P < 0.05$). ‡Significant change in the magnitude of vasoconstriction after propranolol administration ($P < 0.05$).

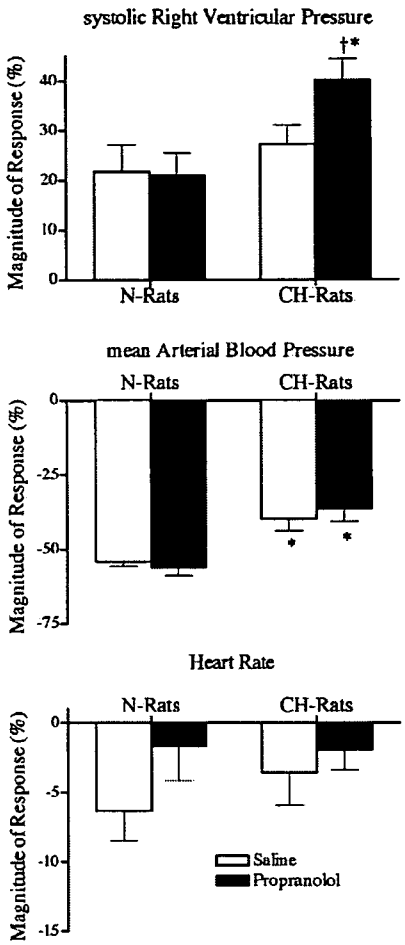

Fig. 6. Hemodynamic responses (% change) of N-rats (n = 5) and CH-rats (n = 5) to acute hypoxia (8% O_2 for 4 min) before and after intravenous administration of propranolol (2 mg/kg). *Significant difference in the magnitude of response between N-rats and CH-rats ($P < 0.05$). †Significant response to propranolol ($P < 0.01$).

underlying mechanisms governing the pathogenesis of PAH remain to be fully elucidated. Specifically, anatomic and structural changes within the pulmonary vascular bed during chronic hypoxia remain unclear.

On the basis of the early work of Reid and colleagues (8, 11, 12, 25), it had become accepted that a reduction in the number of perfused vessels within the pulmonary circulation was an important structural pathology that contributed to the sustained increase in vascular resistance during the pathogenesis of PAH. The reduction in perfused vessels was attributed to either the encroachment of smooth muscle into the vessel lumen, thereby occluding blood flow, or by a reduction in the total number of vessels (i.e., pruning).

One limitation of these studies was the inability to clearly identify the region of susceptibility and the degree of pruning or reduced perfusion. Indeed, because of the limited resolution of conventional X-ray systems, the lung had to first be excised for angiography and then pruning was nonquantitatively described from crude angiographs as a decrease in "background haze" or "background filling" (representing small peripheral vessels) (11, 21, 30).

We (32) have previously described the high definition achieved with SR microangiography for visualizing pulmonary microvessels, with an internal diameter >80 μm. In this study, using SR, we were able to confirm that exposure to chronic hypoxia for 4 wk reduced the number of opaque arterioles with internal diameter >80 μm within the pulmonary circulation. Unlike previous studies, this study was also able to identify the region of susceptibility (i.e., third to fourth generation of branching, 100–300 μm) and to quantify the degree of change (e.g., CH-rats had 47% fewer opaque vessels of the third generation than N-rats) within a closed-chest model, i.e., under intact neurohumoral regulation. One significant limitation with SR, however, is that it is not possible to determine whether the reduction in the number of opaque vessels is due to *1*) pruning of vessels, *2*) occlusion of existing vessels (i.e., complete encroachment of smooth muscle within the vessel lumen), or *3*) partial occlusion, reducing the internal diameter below the resolution limit of SR (i.e., 80 μm).

In the latter case, vessels would still be perfused but would not be visualized by SR. Consequently, the change in the number of perfused microvessels could potentially be overestimated, since we were unable to distinguish between completely occluded and partially occluded vessels. Without further improvements in the signal-to-noise ratio of pixel areas containing fifth-generation branches, it is presently not possible to quantify to what extent the microvessels are perfused in the CH-rat model.

The lung is one of the most densely vascularized organs; therefore, it is extremely difficult to accurately quantify the number of vessels within the "whole" lung. Some studies have claimed that casting techniques, which apply a high-perfusion pressure to distend and fill all arteries to the level of the capillaries, provides evidence that chronic hypoxic reduces vessel number, supporting the concept of pruning (11, 30). However, the reduction of the number of vessels filled with medium within a cast may simply be the result of occlusion, rather than the loss of vessels.

In the past 5 yr, the paradigm of vessel pruning during chronic hypoxia has been challenged, with some reports indicating that the pulmonary circulation appears to undergo angiogenesis during chronic hypoxia (13, 14, 16). However, the vascular region of angiogenesis is uncertain but is likely to occur (if at all) within the capillary bed and/or venules (not the arterioles) because these are the regions of angiogenesis within the systemic circulation (6, 28, 29). Unfortunately, visualizing the capillary network of the lung is presently beyond the resolution capabilities of SR with iodinized contrast agents.

Limitations of this study. Our group has previously described the limitations of SR for visualizing pulmonary vessels <80 μm but also reported that, despite this limitation, a majority of vessels that are susceptible to pathological disorders, and that significantly contribute to an increase in vascular resistance, generally have an internal diameter between 50 and <300 μm (11, 32, 37, 40), i.e., resistance vessels that are at least partially muscular (12). However, resistance vessels <70 μm and lacking complete muscular media also constrict in response to hypoxia (10, 27) and therefore are also likely to be susceptible to pathological changes.

When analyzing the vasoconstriction response to acute hypoxia, we could only analyze vessels with an internal caliber >100 μm because vasoconstriction of vessels <100 μm re-

duced their caliber below the resolution capabilities of SR (i.e., <80 μm).

Another significant limitation of this study is the inability of SR to assess the integrity of the pulmonary arterial vascular wall. Numerous studies have reported that pulmonary vascular remodeling and medial thickening during chronic exposure are significant structural pathologies responsible for the increase in vascular resistance (12, 23, 24, 31). Assessment of vascular remodeling often necessitates histochemical analysis. On the other hand, SR is only able to measure the internal diameter of perfused vessels (assuming the vessel contains sufficient contrast medium) and is therefore a simple, albeit useful, method for assessing gross anatomic changes in the pulmonary circulation of the hypertensive lung. Important information concerning vascular wall thickness and medial thickening cannot be assessed with SR.

In this study, we could not view the circulation of the whole lung; rather, we were restricted to a relatively small field of view of 9.5 × 9.5 mm. We therefore make the assumption that the image captured within the 9 × 9 window is representative of the whole lung circulation. However, changes in vascular resistance (during either acute of chronic hypoxia) are the consequence of global pulmonary vasoconstriction and/or remodeling.

HPV in the rat. In this study, we used SR to assess the dynamic changes in vessel caliber during acute hypoxia (i.e., HPV). The results of this study concur with our previous report (32) that showed, in N-rats, that all vessels with a diameter <500 μm, especially between 200 and 300 μm, constricted in response to acute hypoxia (8% O_2). The unique result of this study is that chronic hypoxia did not significantly alter HPV, as assessed by hemodynamic and microangiography analysis.

HPV has been reported to preferentially occur in vessels with an internal diameter of ~150–300 μm in cats and rabbits (17, 34, 35) and rats (32) and up to 600 μm in dogs (1). Chronic hypoxia has been reported to alter acute HPV due to structural changes in the pulmonary vasculature (22). According to the literature, chronic hypoxia can potentially attenuate (9, 15, 38, 41), enhance, or have no effect on the acute HPV (5, 7, 18). Despite decades of research concerning HPV, the exact mechanism(s) that governs acute HPV is yet to be fully elucidated, although various humoral (e.g., nitric oxide) and neural pathways are likely to be involved [see Moudgil et al. (26) for a review]. In this study, we aimed to specifically assess sympathetic modulation of the HPV by SR microangiography. Although sympathetic fibers innervate the pulmonary vasculature, neural control of "tonic" pulmonary vascular tone is less prominent than that of the systemic vasculature. However, modulation of the pulmonary vasculature by the sympathetic nervous system becomes critically important under stressful conditions, such as hypoxia (33, 35).

Hypoxia is a potent activator of pulmonary sympathetic nerve activity. The increase in sympathetic nerve activity has been reported to attenuate the local vasoconstrictor effects of hypoxia via a β-adrenoceptor-mediated vasodilator mechanism, especially when the inspired level of O_2 is ≤8% O_2 (33, 35). For example, Shirai et al. (35) reported that HPV was greater for moderate (10% O_2) than for severe hypoxia (5% O_2), but only if the hypoxia was global (i.e., whole body). If the hypoxic stimulus was restricted to just the lung (i.e., regional hypoxia), the magnitude of vasoconstriction was proportional to the degree of hypoxia (i.e., greatest for 5% O_2). Shirai et al. (35) subsequently demonstrated that the vasoconstrictor response to severe global hypoxia is offset by a sympathetic β-adrenoceptor-mediated vasodilatory mechanism.

In our study, we observed that sympathetic β-adrenoceptor blockade (using propranolol) in N-rats did not modify baseline vascular tone, but it did accentuate HPV of those vessels 200–300 μm in diameter. These results support the concept that modulation of the pulmonary vasculature by the sympathetic nervous system appears to be an important homeostatic response for limiting the magnitude of vasoconstriction under hypoxic conditions.

Interestingly, although β-adrenoceptor blockade accentuated HPV in this study, it did not significantly alter the magnitude of the systolic RVP to acute hypoxia in N-rats. This difference may be attributed to a decrease in cardiac output (not measured in this study), since β-receptor blockade has been reported to significantly reduce cardiac output (4, 20). Alternatively, the magnitude of vasoconstriction may not have been sufficient to elicit a significant change in the systolic RVP response, since *1*) propranolol accentuated the HPV of only the 200- to 300-μm vessels and *2*) the vasoconstriction observed within the 9.5 × 9.5-mm field of view may not be representative of the whole lung (as discussed above).

The mechanism(s) responsible for alterations of the HPV after chronic hypoxia remains poorly understood. In this study, we observed that β-receptor blockade in CH-rats significantly accentuated the HPV, not only in the 200- to 300-μm vessels as observed in N-rats but also in the 100- to 200-μm vessels. Consequently, the systolic RVP response to acute hypoxia was also enhanced by propranolol. These results indicate that sympathetic modulation of the HPV becomes critically enhanced after chronic hypoxia.

Although the mechanisms for these observations need to be further researched, we speculate that the enhanced HPV may be attributable to *1*) the formation of new muscle around nonmuscular or partially muscular vessels (50–150 μm) and *2*) an increase in sympathetic innervation of the pulmonary vasculature. HPV is intrinsic to the lung, and, although modulated by the endothelium, the core mechanism is in the smooth muscle cell (26). Peripheral arterioles undergo medial thickening during chronic hypoxia. Therefore, in this study, it may be possible that the potential of the 100- to 200-μm vessels to constrict was enhanced after chronic hypoxia. However, the difference in the vasoconstrictive response of 100- to 200-μm vessels between N-rats and CH-rats was only apparent after β-receptor blockade. Studies have shown that chronic hypoxia significantly increases β-receptor number within the lung (3, 39), so that modulation of HPV by the sympathetic nervous system is enhanced after chronic hypoxia. These reports are in agreement with the observations of this study.

Future directions. The primary aim of this study was to demonstrate the effectiveness of SR for "visualizing" the pathological changes in pulmonary microcirculation in a closed-chest rat model after the development of pulmonary hypertension. As a result, this study has provided a foundation with which future investigative studies can build to further elucidate the adverse changes in the pulmonary circulation during hypertension. Specifically, we used only one stimulant (acute hypoxia) to test the reactivity of the pulmonary circulation. However, the question still remains as to whether